A Dual Resonant Microstrip UHF RFID "Cargo Tag" with a CPW Structure for the Feed and Matching Circuit

Supreetha Aroor

Submitted to the Department of Electrical Engineering and Computer Science and the Faculty of the Graduate School of the University of Kansas in partial fulfillment of the requirements for the degree of Master of Science in Electrical Engineering

Thesis Committee:

_____
Chairperson: Dr. Daniel D. Deavours

_____
Dr. James Stiles

_____
Dr. Erik Perrins

_____
Date Defended: 08/22/08

The Thesis Committee for Supreetha Aroor certifies
that this is the approved version of the following thesis:

A Dual Resonant Microstrip UHF RFID "Cargo Tag" with a CPW Structure for the Feed and Matching Circuit

Thesis Committee:

Chairperson: Dr. Daniel Deavours

Dr. James Stiles

Dr. Erik Perrins

Date Approved: 08/22/08

Abstract

The container is at the core of a highly automated system used for moving goods from one geographic location to another. Containers usually contain pallets; pallets contain cases; cases contain items such as pharmaceuticals and electronic goods. Passive UHF RFID has been widely used for tracking goods at the pallet and case-level. Tracking goods at each level can improve efficiency and cut supply chain costs. A practical application for passive UHF RFID is tracking large metal assets such as cargo containers.

In this thesis, we present a high gain, planar microstrip antenna for low-cost RFID tagging of large metal assets. The antenna is dual–resonant and utilizes a coplanar waveguide (CPW) feed structure and matching circuit. The tag can operate over 860-930 MHz, a major portion of the 860-960 MHz frequency spectrum allocated for UHF RFID applications world-wide. We present a rigorous analysis of the antenna along with the circuit model of the antenna which will accurately predict the impedance and performance characteristics. We introduce a polarization model to predict the vertical to horizontal polarization power ratio. The analysis gives insight to the working of the antenna and the feed structure. We present measurement results and data to verify our synthesis of the antenna design. There are still open questions regarding the feed structure of the tag. We model and run several simulation models to provide a better understanding of the feed structure.

Acknowledgment

I would like to thank Dr. Daniel Deavours for giving me the opportunity to work and study in his laboratory, for leading and helping me to complete my thesis. He has encouraged me and prepared me from the very first day. From all the lab meetings, the one to one discussions and the team working, I feel that I have gained a lot since I came into this lab. He has been a wonderful teacher, teaching me both laboratory skills and theoretical approaches with patience and understanding. I am really grateful to him for being my advisor.

I thank Dr. James Stiles and Dr. Erik Perrins for being a part of my thesis committee. A special thanks to Dr. Demarest for his technical insights. I truly appreciate all their suggestions and guidance through the final stages of my thesis.

I would also like to thank ITTC and the EECS department for providing me with this opportunity. I extend my thanks to my fellow graduate students at the RFID Alliance Lab who have helped me in various ways. I extend my appreciation to all my friends who have supported me in many different ways.

Finally, I would like to thank my parents and my brother for all their love and support without which none of this would have been possible.

To my family

Table of Contents

List of Figures

1. Introduction

A cargo container is an aluminum or steel box held together with welds and rivets, with a wooden floor and two enormous doors at one end. The container is at the core of a highly automated system used for moving goods from one geographic location to another and hence an important asset in the supply chain industry. Containers usually contain pallets; pallets contain cases; cases contain items such as pharmaceuticals or electronic goods. Passive UHF RFID technology has been widely used for tracking goods at the pallet and case-level. Tracking goods at each level can improve efficiency and cut supply chain costs. With the Electronic Product Code Gen 2 standards being used all over the world, the industry already has the infrastructure for the technology in place [40]. Passive RFID tags are increasingly being used for asset tracking, which has traditionally been the domain of longer-range-but more expensive-active RFID tags [41].

Containers are carried by ships, trains and trucks all over the country. Container ports are one of the fastest growing business sectors in the U.S. [38]. According to an article in RFID journal, 17,000 containers carrying roughly 80% of U.S. imports arrive daily at U.S. seaports. [39]. Over 8 million containers are loaded or unloaded each year at various U.S. ports [38].

A practical application for passive UHF RFID is tracking large metal assets such as cargo containers. Such metal assets are an ideal application for many reasons: they tend to have a long useful life, allowing the tag cost to be amortized over many uses; the contents change frequently, so associations with a unique

identifier is useful; they frequently cross organizational boundaries, making a common mode of identification useful; and they are physically large, requiring identification at a distance. Also, these containers are shipped between large geographic regions [1].

Inexpensive, passive UHF RFID antennas are typically constructed using stripline dipole antennas [2]. Dipole antennas experience degraded performance when they are placed on or close to metal objects [3] [4] [5] making them unsuitable for tracking large metal assets. Low-profile microstrip antennas which can be used on metal generally have a poor bandwidth [32]. The frequency allocation for UHF RFID is not the same world-wide. Europe predominantly uses 865-869 MHz, North America uses 902-928 MHz and Japan uses 952-954 MHz for UHF RFID applications. Thus, narrow-band microstrip antennas are not well suited for world-wide RFID applications. Also, there is a limitation on the read distance of passive tags. Most of the currently available passive tags in the market do not have the read range required for tracking cargo containers. Therefore, an ideal passive UHF RFID tag for tagging large metal assets such as cargo containers would be a low-cost, long-range tag with a moderate form factor whose operation covers a majority of the world.

In this thesis, we present a high gain, planar microstrip antenna for low-cost RFID tagging of large metal assets. The antenna is dual–resonant and utilizes a coplanar waveguide (CPW) feed structure and matching circuit. Having two resonances, one at 867 MHz and the other at 915 MHz, enables the tag to operate

over 860-930 MHz, a major portion of the 860-960 MHz frequency spectrum allocated for UHF RFID applications world-wide [28]. The tag was found to have a read distance of 60 feet when measured informally. With release of the new Higgs chip, which has a 6 dB improvement over the TI chip used for our design, we can double the read distance. We present a rigorous analysis of the antenna along with the circuit model of the antenna which will accurately predict the impedance and performance characteristics. We introduce a polarization model to predict the vertical to horizontal polarization power ratio. The analysis gives insight to the working of the antenna and the feed structure. We present measurement results and data to verify our synthesis of the antenna design. There are still open questions regarding the feed structure of the tag. We model and run several simulation models to provide a better understanding of the feed structure.

2. Background

In this chapter, we will discuss some of the concepts related to a RFID system and passive UHF RFID. We will introduce previous work where microstrip antennas have been used to solve the metal-water problem. The basics of microstrip antennas, the transmission line model used to analyze microstrip antennas, and coplanar waveguides will be presented. We will also discuss some of the published results made in this field of study.

2.1 RFID System

RFID is an acronym for Radio Frequency Identification. It is technology that uses radio frequency waves to transfer data between a mobile object in order to track, categorize or identify the object. It does not require a line of sight between the reader and the tagged item. The block diagram of a RFID system is shown in the Fig. 1. The RFID system is made of three components: the reader or interrogator, the tag or transponder, and the host computer. The reader is a transceiver connected to receive and transmit antennas on one end and the host computer at the other end.

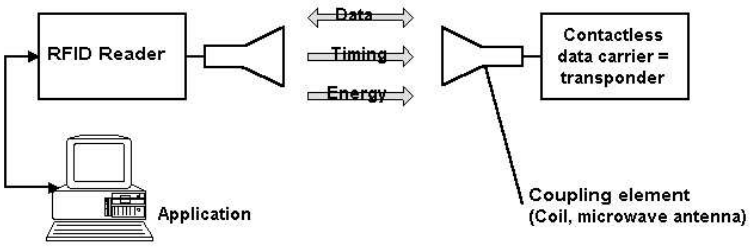

Fig.1 Block Diagram of a RFID system taken from RFID Handbook [25].

The host computer is used to manage the reader, issue commands and to store information received from the reader. The tag consisting of an antenna and the IC, is placed on the object to be identified. Electromagnetic wave propagation enables communication between the tag and the reader. The reader, after getting a command from the host to read the tag, generates a carrier signal and sends the signal to the tag through the reader transmit antenna. The tag modulates the signal and backscatters to the reader through the receive antenna of the reader. The reader decodes the data and communicates the decoded data to the host computer.

2.2 Passive UHF RFID

2.2.1 Operation of passive tags

One very important feature of RFID systems is the power supply to the transponder. *Passive tags* do not have their own power supply and therefore all the power required for their operation must be drawn from the field of the reader [25]. Passive UHF tags operate in the UHF range of the 860 MHz–960 MHz. Different subsets of this range are used in different regions of the world. Table 1 shows the frequency allocated for different countries [28].

In passive UHF RFID systems, the reader transmits RF energy to sense the tag consisting of a tuned antenna and an IC which acts as the load. The tag can be in the near field or far-field of the transmitter. The area after the point where the

electromagnetic field has completely formed is called the far field of the antenna. In this thesis, we deal only with far-field UHF RFID tags.

Table 1: Frequency allocations for different countries

Country	Frequency
Europe	865-869 MHz
USA and Canada	902-928 MHz
Korea	910-914 MHz
Korea and Singapore	923-925 MHz
Hong Kong	920-925 MHz
Japan	952-954 MHz

The antenna receives this power and if there is sufficient energy to power up the IC, the tag responds to the reader. The RF energy from the reader to the tag (forward link) is backscattered from the tag to the reader (reverse link) along with data from the RFID IC.

2.2.2 Maximum Power Transfer

Commonly antennas are designed to match to a substantially real load in order to minimize the standing waves along the transmission line. However, for RFID antennas, the load is in close proximity to the antenna and also reactive. Therefore, in order to maximize the tag performance we must maximize the power transferred to the load (IC).

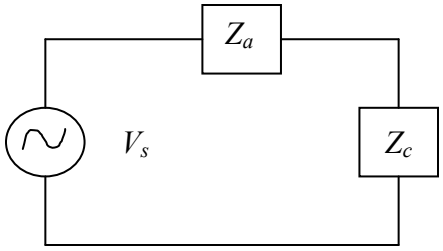

Fig. 2: Circuit model of a RFID tag.

Fig. 2 shows the circuit for a passive RFID tag. Let $Z_a=R_a+jX_a$ and $Z_c=R_c+jX_c$ be the antenna and chip impedance respectively. Maximum power transfer happens when $Z_a=Z_c$*, in which half of the power is transferred to the load and half is scattered [26][27]. The *power transfer efficiency* is the ratio of the actual power transferred to the maximum possible power transferred, which is given by

$$\tau = \frac{4R_a R_c}{|Z_a + Z_c|^2}.$$

A *power wave reflection coefficient* can be defined as

$$s = \frac{Z_c - Z_a^*}{Z_a + Z_c}$$

so that $\tau + |s|^2 = 1$. Here, s plays a similar role to S_{11} in the traditional antenna matching problem. Let

$$\hat{z}_a = r + jx = \frac{R_a}{R_c} + j\frac{X_a + X_c}{R_c}$$

It can be shown that

$$s = \frac{\hat{z}_a - 1}{\hat{z}_a + 1}$$

where *s* is now a Smith chart transformation. The antenna impedance can be plotted on a Smith chart with the distance from $\hat{z}_a$ to the center of the Smith chart being |*s*|. The Smith chart normalized in this way is called the *power wave Smith chart*.

2.2.3 Antenna Characteristics

The ability of the tag to receive RF energy and efficiently backscatter it depends on antenna characteristics and channel properties. Here, we will discuss some of these characteristics; radiation intensity, radiation efficiency, directivity and gain of an antenna.

Radiation intensity in a given direction is defined as the power radiated from an antenna per unit solid angle. The total *power radiated* is obtained by integrating the radiation intensity over the entire solid angle of 4π.

$$P_{rad} = \oiint_{\Omega} U d\Omega = \int_0^{2\pi}\int_0^{\pi} U \sin\theta d\theta d\phi$$

Here, U is the radiation intensity. For an isotropic source, U will be independent of the angles θ and φ. The *directivity* of an antenna is defined as the ratio of the radiation intensity in a given direction from the antenna to the radiation intensity averaged over all directions. The *average radiation intensity* is equal to the total power radiated by the antenna divided by 4π. Therefore, we can define directivity as the ratio of the radiation intensity in a given direction to that of an isotropic source.

$$D = \frac{U(\theta,\phi)}{U_0}$$

We can see that this is a unitless quantity.

If an antenna is considered as a device that accepts power from one device and radiates it into space, then the *radiation efficiency* of an antenna can be defined as the ratio of power radiated into space to the total power accepted [6][7]. It is also known as *antenna efficiency*, η.

$$\eta = \frac{P_{radiated}}{P_{accepted}}$$

The antenna cannot re-radiate all the power accepted by it. Some of the power is lost due to heat or dielectric losses or absorption from the ground. As mentioned before, maximum power transfer is achieved when the antenna impedance is the complex conjugate of the chip impedance. Therefore, a tag antenna can have good radiation efficiency and still be poor in performance if there is considerable mismatch between the load and the antenna impedance. A mismatch will result in RF energy being reflected back to the transmitter without powering up the RFID IC.

We can define gain of the antenna which takes both the radiation efficiency and the impedance match into account. By definition [6], the *gain of an antenna* is the ratio of the energy radiated in particular direction when the antenna is excited with a certain amount of input power to the theoretical isotropic antenna excited with the same amount. The directivity, gain and efficiency are related as:

$$G(\theta,\phi) = \eta D(\theta,\phi)$$

Gain is also a unitless quantity. It is usually expressed in dB. We can see from the above equation that for a radiator whose efficiency is 1, the gain is equal to the

directivity. However in most cases, the efficiency is less than 1, and the gain is usually less than the directivity.

2.2.4 Friis Transmission Equation

Assuming that the RFID system is operated in an ideal channel environment, Friis equations [6][8] can be used to determine the power received from the reader to the tag for a given distance. Therefore, if the tag antenna is the receiving antenna and the reader antenna is transmitting and the two are separated by a distance '*r*',

$$P_r = \frac{P_t G_t G_r \lambda^2}{(4\pi r)^2}$$

where P_r is the power received from reader antenna to the tag antenna. P_t is the power transmitted by the reader. The reader and tag antenna gains are given by G_t and G_r respectively. However, there could be polarization mismatch (ρ) between the reader and the tag antennas, and also not all the power absorbed by the receiver is available to the load due to impedance mismatch (τ). Taking these factors into consideration the modified Friis equation is written as shown in equation:

$$P_r = \rho\tau \frac{P_t G_t G_r \lambda^2}{(4\pi r)^2}.$$

The received power is used to power up the RFID IC and re-radiate to the reader.

2.3 Performance degradation of Passive UHF RFID tags

Inexpensive, passive UHF RFID antennas are typically constructed using stripline dipole antennas [2]. The antennas are usually electrically short and narrow in order to minimize the cost. RFID tags perform well in free space [23], but undergo performance degradation when attached to different materials [24]. Dipole antennas experience degraded performance when they are placed on or close to metal objects [5]. RFID tags degrade in their performance when placed near high dielectrics such as water. This loss of performance is because the material characteristics affect critical antenna properties such as substrate dielectric constant and loss tangent, radiation efficiency, radiation pattern, and radiation impedance. This problem is called the "metal-water" problem. However, many metal assets need to be tracked and a solution to this problem is imperative.

Active RFID systems offer an alternative to this, but are considerably more expensive. Several attempts [9][10][11] have been made to create UHF RFID tags that perform well when attached to metal or plastics. They are mostly, specific models that are pre-tuned to work on different materials [10][11]. For example a tag designed to work well near metal will still be de-tuned when placed on plastic or near water. Another solution is to encase ordinary dipoles in rugged plastic cases to shield them from the effects of metal or water. One way to achieve uniform performance with different materials is to design an antenna that is electrically separated from the material on which the tag is placed. Microstrip antennas can provide a solution to this problem.

2.4 Microstrip Antenna: Solution for the Metal-Water Problem

Microstrip "patch" antennas are a well known class of antennas. A microstrip antenna consists of: the primary radiating element ("antenna"), a dielectric substrate, a ground plane and a feeding element. The ground plane separates the microstrip antenna from the material to which it is attached. There are numerous substrates that can be used to construct microstrip antennas. Common feeds include a probe feed from a coaxial cable or edge feed with a microstrip transmission line, although proximity feeds and coupling through a slot in the ground plane are also possible.

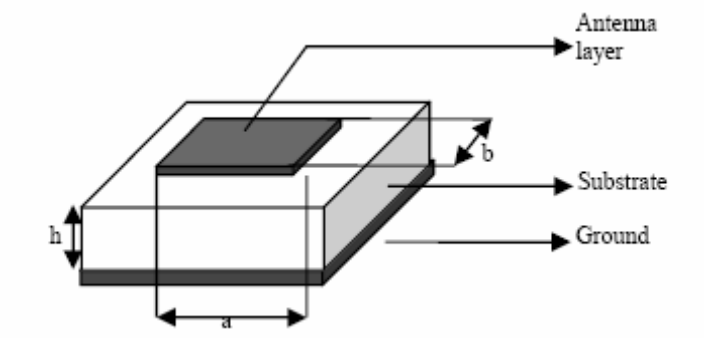

Fig. 3: Rectangular microstrip antenna.

Fig. 3 shows a rectangular microstrip antenna. Microstrip patch antennas radiate primarily because of the fringing fields between the patch edge and the ground plane. Since the propagating EM fields lay both in the substrate and in free space, a quasi-TEM mode is generated. The length and width of the patch are given by a and b respectively. The substrate thickness is given by h. When a > b, the TM_{10} mode is the fundamental resonant mode and TM_{01} is secondary. If dimension along b > a, then the TM_{01} mode is the fundamental resonant mode and the TM_{10} is the secondary

mode. Microstrip antenna designs, however, suffer from manufacturing complexity since most microstrip designs use feed techniques that require connection between the antenna layer and the ground plane. The traditional techniques used for constructing matching networks is by a cross-layered structure, such as a via or a shorting wall. Cross-layer structures require more complex and costly construction.

In [12], a completely planar microstrip RFID tag design is presented. This implementation does not require any cross-layered structures and hence greatly simplifies tag construction. The new antenna and the matching circuit design using the balanced feed approach eliminates the need for a via to the ground [12]. Fig. 4 shows a balanced feed microstrip antenna.

Fig. 4: FCC Planar Microstrip RFID antenna-top view [taken from 12].

We will use this balanced feed approach for constructing a completely planar microstrip antenna. A challenge with microstrip antennas is that they have a narrow bandwidth and a single resonant frequency. This poses a problem for our application since we need a RFID tag which can operate over a wide frequency band.

2.5 Analytic Model- The Transmission Line Model

There are many methods of analysis for microstrip antennas. The most widely-used models are the transmission line model, the cavity model, and the full-wave method. The transmission-line model is one of the simpler methods to analyze a microstrip antenna. It provides good physical insight and accurately models the input impedance. However, it is less accurate than the other models and it is difficult to model coupling of transmission lines with this model. The cavity model is more complex than the transmission line model and has been accurately used to model coupling [13][14][15]. The full wave models are the most accurate and versatile. They are also the most complex and give less physical insight. In this section, the transmission line model of a rectangular patch is discussed in detail. The *transmission line model* basically represents the microstrip antenna by two slots separated by a transmission line with low characteristic impedance and a length L.

2.5.1 Fringing fields

A rectangular patch has finite length and width. Due to this, the fields at the edges undergo fringing. The amount of fringing is dependent on the dimensions of the rectangular patch and the height of the substrate. Fringing is a function of the width of the patch, the height of the substrate and the dielectric constant of the substrate. During analysis, fringing must be considered as it affects the resonant frequency of the antenna.

Fig. 5 shows a microstrip line and typical electric field lines of a microstrip line. It can be considered as a non homogenous transmission line of two dielectrics: air and substrate. ε_r is the dielectric constant of the substrate. Some of the electric field lines exist in the air and some of them are in the substrate. Most of them are in the substrate as can be seen in the figure. In order to account for the fringing and the wave propagation in the microstrip line, it is necessary to define an effective dielectric constant.

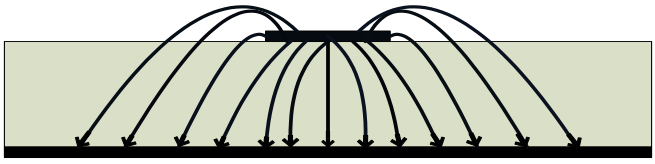

(a) Fringing fields

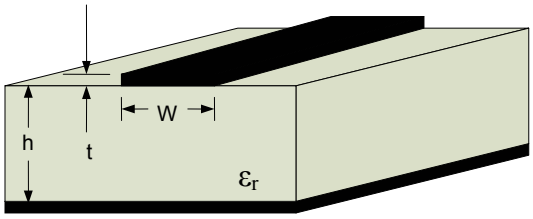

(b) microstrip line

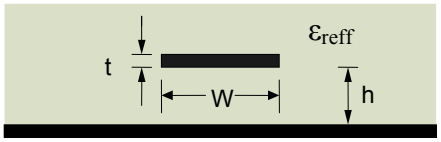

(c) effective dielectric

Fig. 5: Microstrip line and its electric field lines, and effective dielectric constant geometry [6].

The effective dielectric constant is determined by assuming that the center conductor of the microstrip line is embedded into one dielectric as shown in the figure. The effective dielectric constant, $\varepsilon_{reff,}$ is defined as the dielectric constant of the uniform dielectric material so that the microstrip transmission line of Figure 5(c) has the same propagation constant as the actual microstrip line of figure 'a' [6].

Usually, we find that $1<\varepsilon_{reff}<\varepsilon_{r.}$ If the dielectric constant of the substrate is greater than one then the effective dielectric constant is close to the value of ε_r. The effective dielectric is also a function of the frequency. As the frequency increases, the effective dielectric comes closer to the value of ε_r. At low frequencies, it is almost a constant.

2.5.2 Feeding Mechanism

There are several methods for feeding a microstrip patch antenna. There are direct feeding mechanisms such as microstrip line feed and coaxial probe feed and coupled feeding mechanisms such as aperture coupling and proximity coupling. In this work, we use direct feeding mechanisms similar to the microstrip line feed. The microstrip line feed is a conducting strip, usually having a much smaller width than the rectangular patch. It is easy to fabricate and simple to model. The microstrip line is directly connected to the edge of the patch. By feeding at an inset position, the input resistance can be decreased. In subsequent sections, we will discuss more about this feeding mechanism; how it can be modeled and how the inset position affects the resistance.

2.5.3 Radiating Conductance

A rectangular microstrip patch and its equivalent circuit transmission line model are illustrated in Fig. 6.

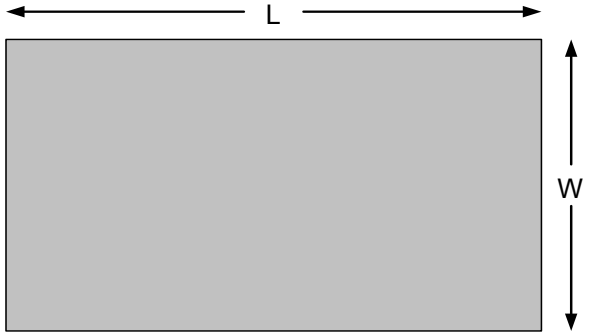

(a) Rectangular patch

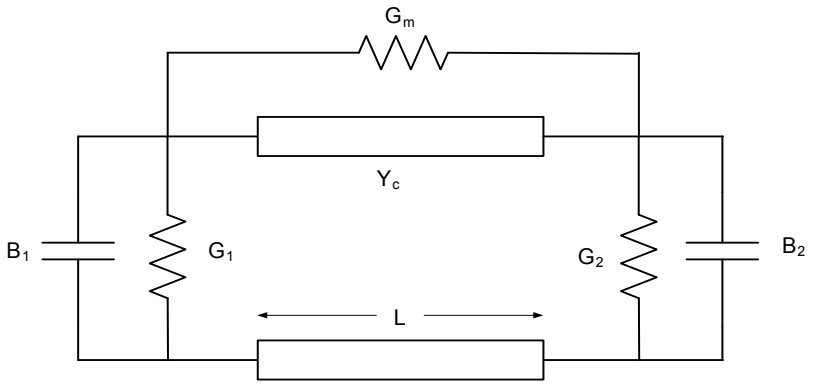

(b) Transmission line model

Fig. 6: Rectangular patch and its equivalent circuit transmission line model.

Each radiating edge can be modeled as a parallel RC combination. Since both edges are identical, the value of the edge conductances are the same and the asymptotic value is given as [18]:

$$G_1 = \begin{cases} \dfrac{1}{90}\left(\dfrac{W}{\lambda_0}\right)^2 & W << \lambda_0 \\ \dfrac{1}{120}\left(\dfrac{W}{\lambda_0}\right) & W >> \lambda_0 \end{cases}$$

where λ_0 is the freespace wavelength.

There is also mutual conductance between the radiating edges or slots. The mutual conductance is defined in terms of far field zones and it can be shown that it can be calculated using [16][17]

$$G_{12} = \frac{1}{120\pi^2}\int_0^{\pi}\left[\frac{\sin\left(\frac{k0W}{2}\cos\theta\right)}{\cos\theta}\right]^2 J_0(k_0 L\sin\theta)\sin^3\theta d\theta$$

2.5.4 Input resistance

The total admittance at one radiating slot is determined by transforming the admittance at the other radiating slot using admittance transformation equations of transmission lines [13]. The length of the patch is *λ/2* for resonance if the dielectric is air. There is usually a substrate with a dielectric greater than one present. Due to fringing the actual separation might be slightly less than λ/2. However, if we approximate that the separation is close to *λ/2*, then Fig. 7 shows the circuit model after a λ/2 transformation.

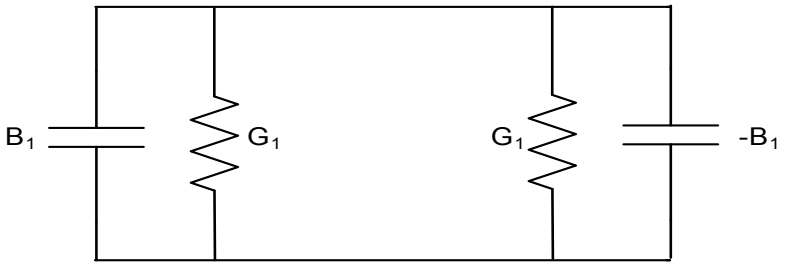

Fig. 7: Transmission line model after λ/2 transformation.

The admittance at the second slot is now G_1-jB_1. The total resonant input admittance is real and is given by

$$Y_{in} = G_1 + jB_1 + G_1 - jB_1 = 2G_1$$

The total input resistance at resonance is given as

$$Z_{in} = \frac{1}{Y_{in}} = R_{in} = \frac{1}{2G_1}$$

The above equation does not take into consideration the mutual conductance. Including the mutual conductance between the radiating slots in the equation for the input resistance, we get

$$R_{in} = \frac{1}{2(G_1 \pm G_{12})}.$$

2.5.5 Input Resistance for an Inset feed

The input resistance calculated above is at the edge of the rectangular patch. Using an inset feed, we can decrease the input resistance. The inset feed is recessed at a distance y_0 from the edge. Fig. 8 shows a rectangular microstrip with a recessed microstrip-line feed.

Using modal-expansion analysis, the input resistance for the inset feed is given approximately by [13][16]

$$R_{in(y=y_0)} = R_{in(y=0)} \cos^2\left(\frac{\pi y_0}{L}\right)$$

where,

$$R_{in(y=0)} = \frac{1}{2(G_1 + G_{12})}$$

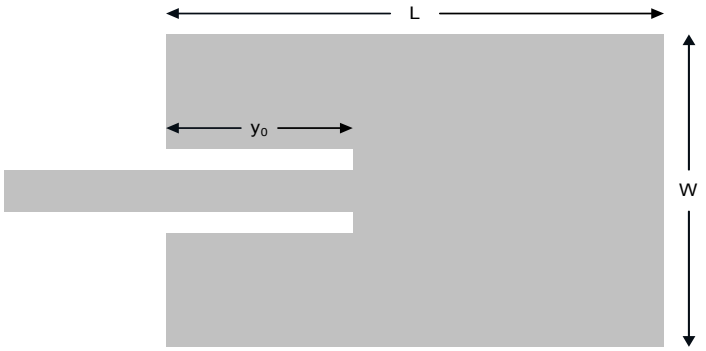

Fig. 8: Recessed Microstrip line feed.

We discuss in Chapter 4 about how this equation can accurately model the input resistance at the inset feed point but not the resistance seen at the input of the microstrip line feed, i.e, the resistance transformed by the microstrip line feed.

2.5.6 Quality factor

The quality factor, bandwidth and efficiency are antenna figure of merits and are all interrelated. It can be difficult to optimize all of them. Therefore, there is a trade off in performance. So we often optimize one of them while reducing the performance of the other.

The *quality factor* is a measure of the antenna losses [6]. Lower the loss, higher the quality factor, Q. It tells us the rate at which energy is dissipated.

$$Q = 2\pi \frac{energy\ stored}{energy\ dissipated\ \ per\ cycle}$$

Typically, there are four kinds of losses that can occur. They are: radiation, conduction (Ohmic), dielectric, and surface wave losses. The total quality factor is influenced by all of these losses and is given by their sum. It can be derived as follows:

Assuming that the total energy stored (W_s) remains a constant, we can write

$$\frac{1}{2\pi}\frac{W_t}{W_s} = \frac{1}{2\pi}\frac{W_{rad}}{W_s} + \frac{1}{2\pi}\frac{W_c}{W_s} + \frac{1}{2\pi}\frac{W_d}{W_s} + \frac{1}{2\pi}\frac{W_{sw}}{W_s}$$

where W_{rad} is the energy dissipated due to radiation, W_c is the energy dissipated due to conduction, W_s is the energy dissipated due to dielectric loss and W_{sw} is the energy dissipated due to surface waves. Therefore, we can write,

$$\frac{1}{Q_t} = \frac{1}{Q_{rad}} + \frac{1}{Q_c} + \frac{1}{Q_d} + \frac{1}{Q_{sw}}$$

where Q_t is the total quality factor, Q_{rad} is the quality factor due to radiation losses (space wave losses), Q_c is the quality factor due to conduction losses, Q_d is the quality factor due to dielectric losses and Q_{sw} is the quality factor due to surface wave losses.

For thin substrates the losses due to surface waves can be neglected. Also, for thin substrates when $h<<\lambda_0$, approximate formulas can be used to represent the quality factors of various losses [13]. They are given below.

$$Q_c = h\sqrt{\pi f \mu \sigma}$$

$$Q_d = \frac{1}{\tan\delta}$$

$$Q_{rad} = \frac{2\omega\varepsilon_r}{hG_t / l}K$$

where, tan δ is the loss tangent of the substrate material, σ is the conductivity of the conductors associated with the patch and ground plane, $G_t / l = G_{rad} / W$ is the total conductance per unit length of the radiating aperture and K=*l*/4 for a rectangular aperture. Therefore, the quality factor due to radiation loss is inversely proportional to the height of the substrate and the thinner the substrate, the more dominant it gets.

2.6 Circuit Model for a Microstrip Antenna

A rectangular microstrip antenna can be modeled as parallel RLC circuit. A microstrip line feed or a probe feed of a short length can be modeled as an inductor. The circuit model of a microstrip antenna with a microstrip line feed is shown below:

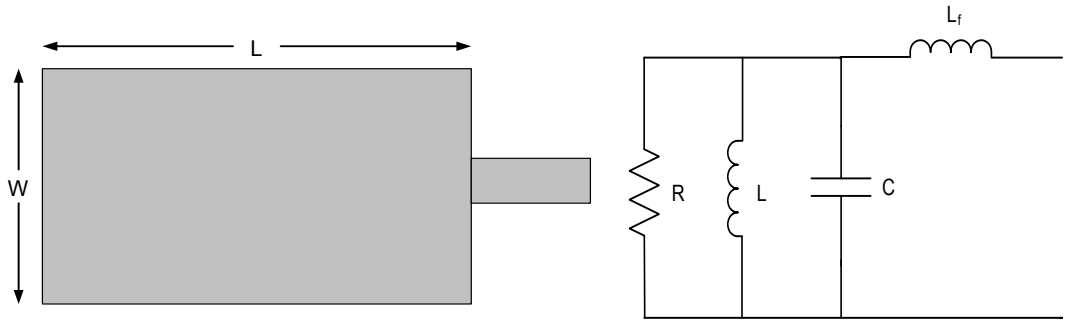

(a) Rectangular microstrip fed with a microstrip line (b) Circuit model equivalent

Fig. 9: Rectangular microstrip with feed and its circuit model equivalent.

We will first verify that the rectangular patch can be modeled as a parallel RLC by comparing simulation results with the circuit analysis results. Next, we will modify the transmission line equation for input impedance to find the value for the inductor used to model the feed.

2.6.1 Analysis

To show that a rectangular microstrip antenna can indeed be modeled as a parallel RLC circuit, we ran a simulation of the impedance of a rectangular patch antenna with a lumped port using a finite element method simulation tool as shown in Fig. 10.

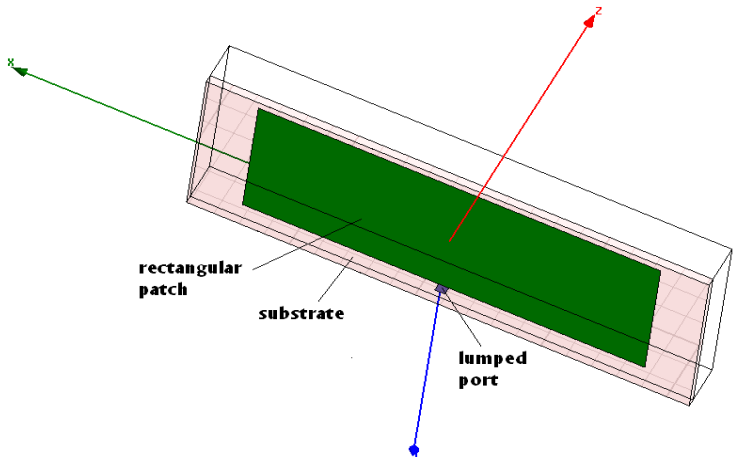

Fig.10: HFSS model of rectangular microstrip. The ground plane is below the substrate.

The impedance graph was generated using the same finite element method tool and it is given in Fig. 11. Next, the impedance graph of a parallel RLC circuit with R=30 ohms, L= 70 pH and C= 125 pF having a resonance at 1.75 GHz is given in the Fig. 12. The resonant frequency can be calculated using the formula below.

$$f_0 = \frac{1}{2\pi\sqrt{LC}}$$

The quality factor of a parallel RLC circuit is given by:

$$Q = \frac{R}{\sqrt{\frac{L}{C}}}$$

We can see that the two graphs are nearly identical. By adjusting the resistance, the Q and the values of inductance and capacitance, the two graphs can be made identical. Hence, a rectangular microstrip patch can be modeled as a parallel RLC circuit near resonance.

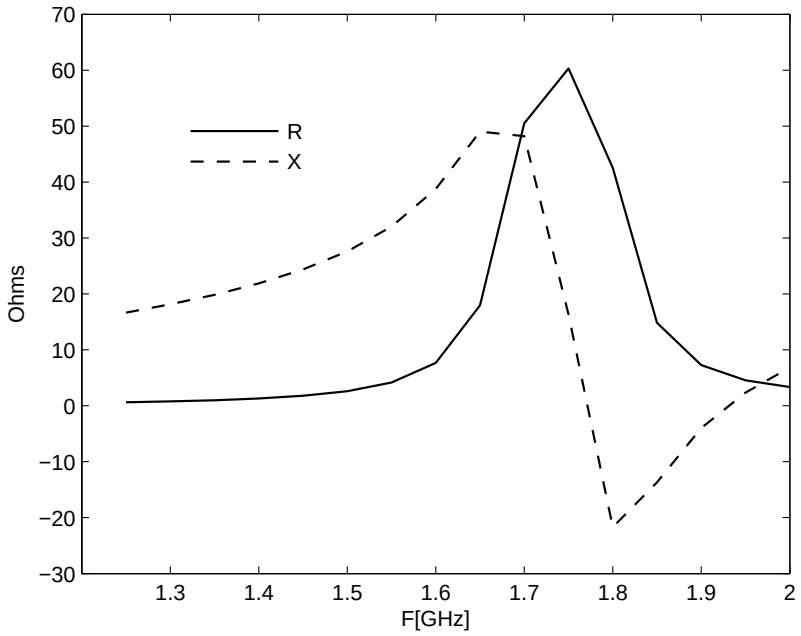

Fig.11: HFSS simulation graph of impedance vs frequency of microstrip patch.

.

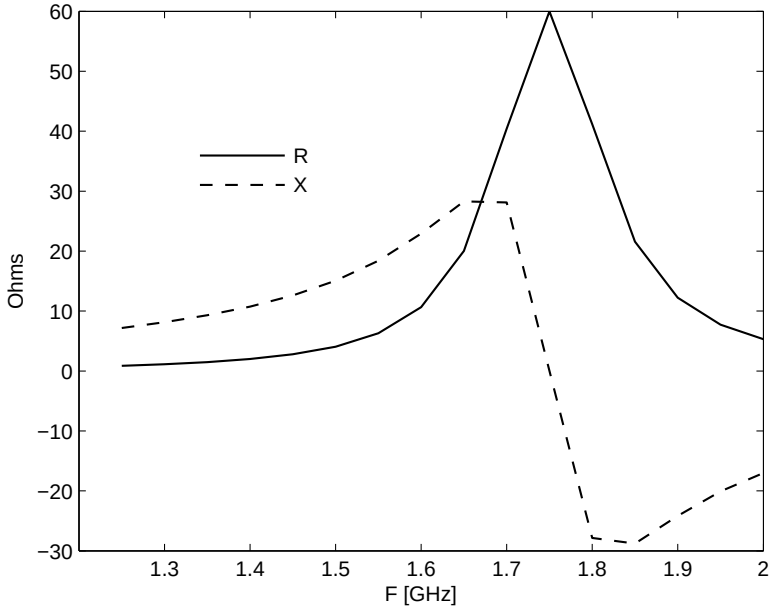

Fig. 12: Impedance vs Frequency of a parallel LRC circuit.

A microstrip line feed can be modeled as an inductor. The microstrip line maybe considered as a short transmission line. In the next section, starting from the input impedance of a transmission line, we derive the inductance.

2.6.2 Transmission Line Equivalence

The input impedance of a transmission line is given as:

$$Zin = Z_0\left[\frac{Z_l + jZ_0 \tan \beta l}{Z_0 + jZ_l \tan \beta l}\right]$$

For a short transmission line , Z_0 , the characteristic impedance of the transmission line, is very high and $Z_l << Z_0$

$$Zin = Z_l + jZ_0 \beta l$$

where Z_l is the feed impedance and $jZ_0\beta l$ is the inductance of the inductor used to model the microstrip line feed.

2.7 Coplanar Waveguide

2.7.1 Description

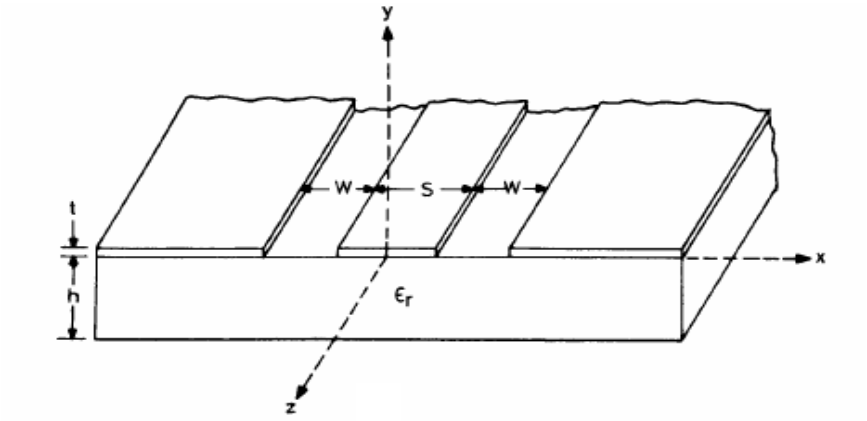

Fig. 13: Coplanar Waveguide Structure [Taken from 19].

The coplanar waveguide was proposed by Wen [22] in 1969. It consists of two slots of width W printed on a dielectric substrate as shown in Fig.13. The spacing between the slots is denoted by S. The conventional coplanar waveguide introduced by Wen cannot be used as such because of the requirement of infinitely thick substrate. For practical purposes, substrate thickness has to be finite. Also, the ground planes of actual CPW have finite widths and should be kept as small as possible. The fields of a CPW are less confined than those of microstrip lines, thereby making them more sensitive to covers or shields placed over the guide. It is tempting to introduce a conductor backing to improve both the mechanical strength and the power handling

capability. Moreover, it allows easy implementation of mixed CPW-microstrip circuits. There are different variations of CPW, such as CPW with and without ground planes, asymmetric CPW where the width of one slot is different than the other. In the following section, we will analyze a CPW with a ground plane.

2.7.2 Analysis of Coplanar Waveguide with a ground plane

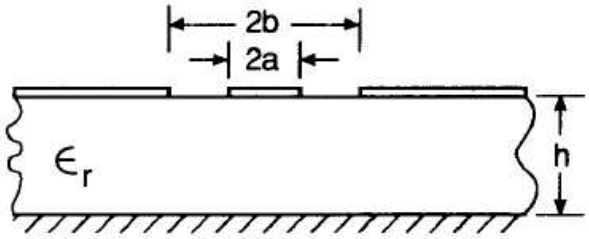

Fig. 14: Coplanar Waveguide with a ground plane [Taken from 19].

Fig. 14 shows a coplanar waveguide with a ground plane (also called conductor-backed CPW). CPWs have been analyzed using the quasi-static approximation. Wen[22] studied these transmission lines using conformal mapping, with the assumption that the dielectric substrate is thick enough to be considered infinite. Conformal transformation has also been applied to take into account the effects of the finite thickness of the dielectric substrate, finite size of the ground planes, ground plane below the substrate, structural asymmetry and multilayer configuration [19].

The assumption in the analysis is that all the interfaces in the structure can be replaced by magnetic walls. For, analysis purposes, the structure in divided into two halves, one above and one below the metallization. Capacitance per unit length is determined transforming it into a parallel plate geometry using conformal transformation. These capacitances yield the characteristics of the line. The expressions given below for the characteristic impedance and effective dielectric constant of a CPW with ground are based on the quasi-static analysis and the conformal transformation [19].

The effective dielectric constant of the CPW is given by:

$$\varepsilon_{re} = 1 + q(\varepsilon_r - 1),$$

where q is the filling fraction. For a conductor-backed CPW, the filling fraction can be calculated using the equation below:

$$q = \frac{K(k_6)/K'(k_6)}{K(k_1)/K'(k_1) + K(k_6)/K'(k_6)}$$

where,

$$\frac{K(k)}{K'(k)} = \frac{\pi}{\ln[2(1+\sqrt{k'})/(1-\sqrt{k'})]} \quad \text{for } 0 \le k \le 0.707,$$

$$\frac{K(k)}{K'(k)} = \frac{1}{\pi}\ln[2(1+\sqrt{k'})/(1-\sqrt{k'})] \quad \text{for } 0.707 \le k \le 1,$$

$$k_1 = a/b,$$

$$k_6 = \frac{\tanh(\pi a/2h)}{\tanh(\pi b/2h)}.$$

The characteristic impedance can calculated using

$$Z_{0cp} = \frac{60\pi}{\sqrt{\varepsilon_{re}}} \frac{1}{K(k_1)/K'(k_1) + K(k_6)/K'(k_6)}.$$

An advantage of conductor-backed CPW is that it improves the mechanical strength of the transmission line so that thin substrates can be used. However, conductor backing reduces the line impedance considerably.

2.8 Dual-resonance

Dual- frequency antennas are antennas which resonate at two frequencies. Dual-resonant microstrip antennas have been studied since many years. Many designs have been discovered.

2.8.1 Dual Resonant rectangular patch antenna

In [20], a simple design a rectangular patch with a coaxial feed is presented. The frequencies of operation are determined from the rectangular patch dimension and substrate dielectric. The feed position is chosen such that both the TM_{01} and TM_{10} modes are excited. Fig.15 shows the rectangular patch along with the selection point for dual frequency operation of the antenna.

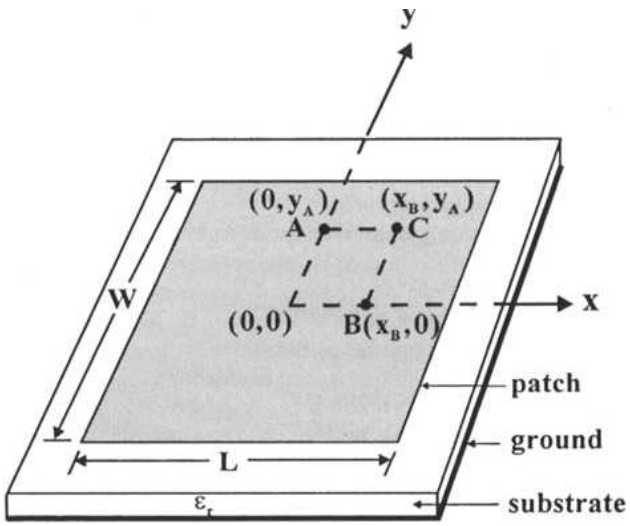

Fig. 15: Selection of the feed position for dual frequency operation; point A for TM_{01}; point B for TM_{10} and point C for dual-frequency operation [Taken from 20]

Using the cavity model approximations, the resonant frequencies for the TM_{mn} modes can be calculated using

$$f_{mn} = \frac{c}{2\sqrt{\varepsilon_r}}\sqrt{\left(\frac{m}{L}\right)^2 + \left(\frac{n}{W}\right)^2}\ .$$

Dual resonance is excited when feeding the patch along the diagonal at point C shown in Fig. 15.

2.8.2 Rectangular patch antenna with cross slots

In section 2.7, we discussed that a microstrip antenna can be made dual resonant by feeding it along the diagonal. In [21], a dual resonant microstrip antenna is presented with reduced dimensions. The dimension of the rectangular patch can be

reduced by placing cross slots at the center of the patch. This makes it electrically longer by increasing the path of the currents as shown in Fig. 16. Hence, the resonant frequency is reduced and we can obtain a resonant frequency with a reduced dimension.

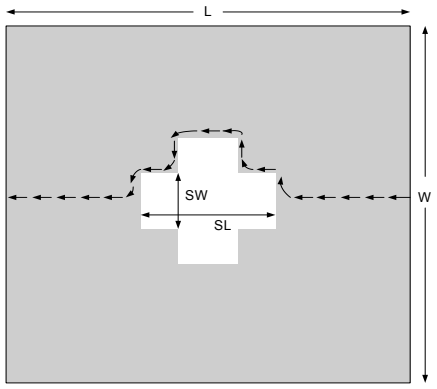

Fig: 16: Path of currents on a rectangular patch with cross slot

3. Initial Design

The inspiration for the design comes from a combination of three factors. First, from the dual-resonant rectangular antennas closely exciting the TM_{01} and TM_{10} modes and feeding in such a way to excite both modes [20]. Second, we draw from the use of microstrip transmission lines to build a completely planar microstrip antenna [12]. Third, we note the use of a cross-shaped slot in a microstrip antenna originally used to reduce the size of the antenna [21], but instead we use the cross as space to place the matching circuit and IC. The slots can also be used to resize the antenna as necessary to control the form factor. In [1], such a design is presented and in this section we discuss the design and measurements in detail.

3.1 Implementation

Fig. 17 shows the antenna geometry. The darkened area represents the metalized area. The antenna was designed to operate over a polypropylene substrate 5.08 mm thick having a dielectric constant of 2.28 and a loss tangent estimated to be 0.001. The substrate and ground plane are 6 inches (15.2 cm) square. A finite element method synthesis tool was used to simulate the design. The initial design to use a simple cross resulted in a matching circuit with a reactance that was too large for our IC (13-*j*65 Ohms). To reduce the reactance, we shortened the transmission lines in the matching circuit by imposing a diamond-shape cut-out within the cross. The cross segments have a length of 34 mm and width of 8 mm. The diamond is approximately

19.8 mm per side. The center of the feed lines is 15 mm from the center, with width 2 mm in order to achieve the desired input resistance. The length of the feeds can be adjusted to achieve a reactance of approximately j65 Ohms at resonance. The matching circuit was designed to obtain a perfect conjugate match to 13−j65 Ohms at 867 MHz, and a slightly larger real resistance at 915 MHz to achieve larger bandwidth. Having had experience in designing microstrip antennas using a finite element tool and utilizing some fundamental concepts, following are some guidelines for designing the antenna from a high level understanding:

- The resonant frequency can be decreased or increased by increasing or decreasing the length of the antenna respectively
- The resonant frequency can be decreased or increased slightly by increasing or decreasing the slot lengths respectively.
- Matching to a larger or smaller resistance is achieved by placing the feedlines further apart or closer together, respectively.
- If the resistance is too small, the size of the cross may need to be expanded to facilitate a larger R_a.
- A smaller X_a can be achieved by shortening the feed lines, and a larger X_a by longer feed lines.
- Keeping the length of the feed line constant, a smaller X_a can be achieved by increasing the width of the feed line and a larger X_a by decreasing the width of the feed line.

When the first resonant mode is excited, one of the feeds acts as an inset microstrip feed, while the other feed lies primarily along the axis of symmetry and thus acts as a feed from an electrical reference, i.e., the virtual ground.

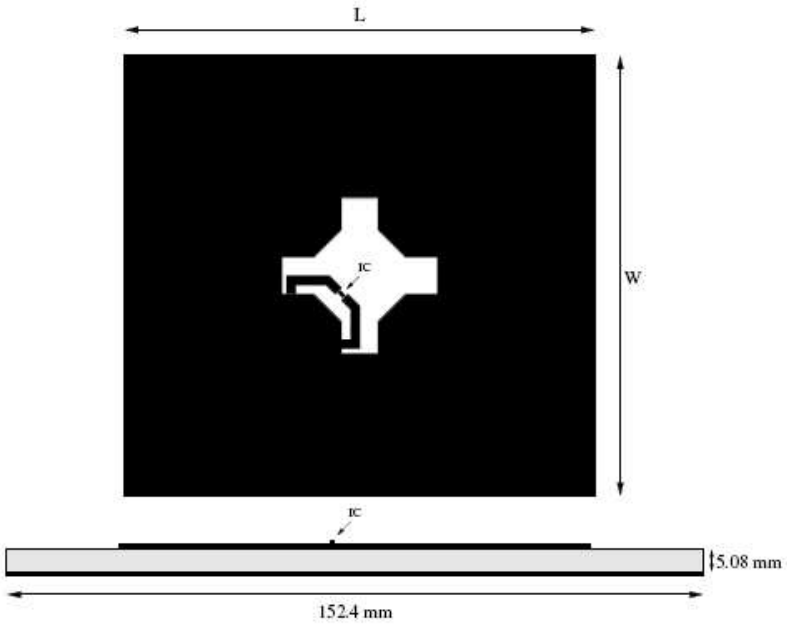

Fig. 17: Antenna geometry of the dual-resonant microstrip RFID tag

When the second mode is excited, the role of the two feeds reverse. Fig. 18 shows the simulated impedance results. We can see that there are two resonances. The two resonant frequencies can be easily adjusted by adjusting L and W. Here, we present resonant frequencies of 867 and 915 MHz using L = 103 mm and W = 97 mm. To achieve resonant frequencies of 915 and 953 MHz, we can set L = 97 mm and W = 92.5 mm. For resonant frequencies at 867 and 953 MHz, we can set L = 103 mm and W = 92.5 mm. In this way, the antenna can be adjusted to work at any two of the three major frequencies of operation worldwide and with most commercially-available RFID ICs.

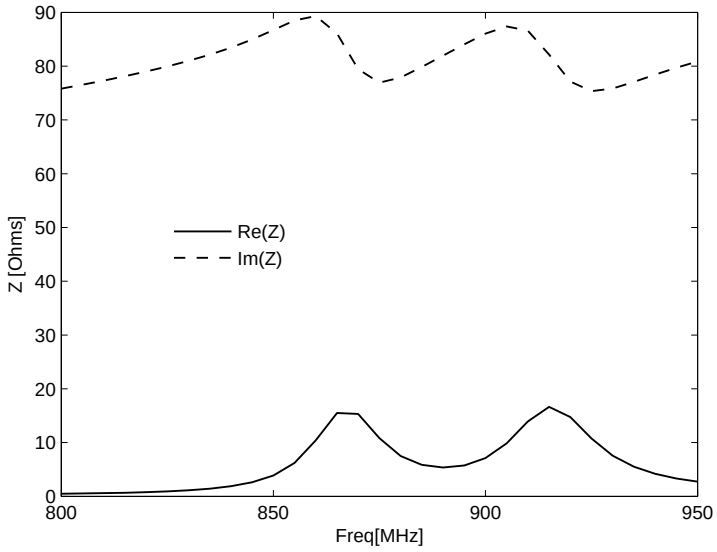

Fig. 18: Impedance vs Frequency

Fig. 19 illustrates the simulated currents on the antenna at the two resonant frequencies. One can see that the TM_{01} and TM_{10} modes are clearly excited with only a minor diagonal component excited at each frequency.

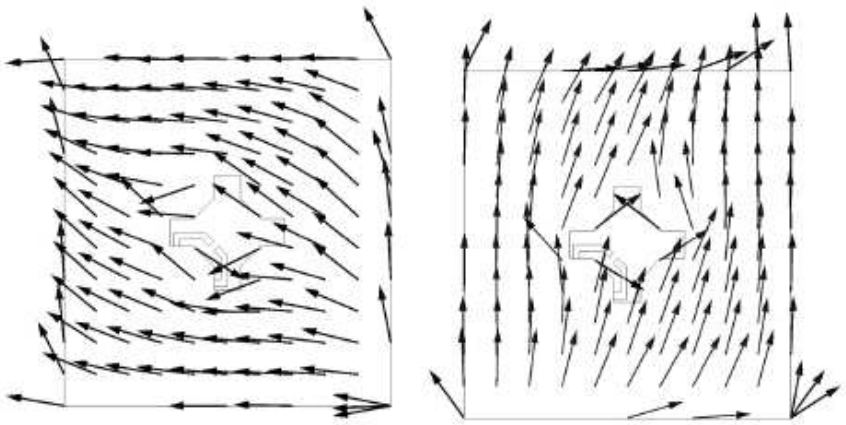

Fig.19: Simulated currents on the antenna

3.2 Measured Results

As the antenna impedance is considerably reactive and balanced, it is difficult to use standard microwave measurement techniques. Since the antenna has a balanced feed, we cannot directly measure the impedance using a network analyzer. We need a balun to convert the balanced feed to an unbalanced feed. We constructed a measurement apparatus using a 1:2 chip balun to measure the impedance using a network analyzer. The balun is mounted on a small PCB that converts a SMA signal to a differential signal to short pins. The unbalanced end is connected to the network analyzer and the balanced end is used to probe the antenna IC pads. Before taking measurements, the network analyzer with the balun is calibrated using short open and a 100 ohm resistor to remove any system inaccuracies. Since we use a 100 ohm resistor, the results obtained must be doubled. The apparatus yields only modest accuracy, but sufficient for the purpose here. The impedance measurements were taken over the range of 830 to 960 MHz. Also, since the impedance is near the edge of a 50 Ohm Smith chart, the accuracy of the network analyzer is likely to be relatively poor. The power wave Smith chart (Section 2.2.2) using the normalized impedance $13 - j65$ is plotted in Fig. 20

Note that we are able to achieve an almost perfect conjugate match at 870 MHz. The 90% transfer efficiency spans between 864 and 875 MHz, and between 915 and 930 MHz. At 900 MHz, τ = 70%. By making the antenna slightly less inductive, the 1 dB bandwidth would span between 860 and 940 MHz, and the 3 dB bandwidth would cover from less than 830 to more than 960 MHz.

The simulated results of the antenna using a finite element analysis code [30] indicates a directivity of 6.2 and 6.1 dBi and radiating efficiency of −0.36 and −0.31 dB at 870 and 915 MHz, respectively. The measured impedance indicates $\tau \approx 0$ dB at 870 MHz and -0.4 dB at 915 MHz. Combining terms, we would expect a realized gain (the product of antenna gain and power transfer efficiency) of 5.9 and 5.4 dBi, respectively.

The free-space Friis equation can be modified for RFID transponders [29].

$$r = \frac{\lambda}{4\pi}\sqrt{\frac{P_t G_t G_r \tau \rho}{P_{th}}}$$

Here, the subscript '*t*' represents the transmitter (reader) and the subscript '*r*' represents the receiver (tag); τ is the power transfer efficiency, ρ is the polarization mismatch, and P_{th} is the minimum (threshold) power to operate the IC. Commonly, readers use 6 dBi circularly polarized antennas and tag antennas are linearly polarized, leading to a polarization loss of 0.5. Using a published value of $P_{th} = -13$ dBm [31], the maximum read distance of the tag from a commodity reader with $P_t =$ 30 dBm and $G_r = 5.4$ dBi is approximately 9.7 meters (32 feet). Utilizing a 3 dB ground reflection, one could expect 13.7 meters (45 feet).

An informal read distance experiment was performed outdoors in an open field. The tag was first affixed to an expanded polystyrene sheet and held approximately one meter above the ground and far from any other object. We used a commodity reader (Mercury 4) at maximum FCC power settings (36 dBm EIRP-Effective Isotropic Radiated Power) with a bistatic circularly polarized antenna. The

tag was moved away from the reader until we found the maximum distance at which the tag was detectable (maximum detectable distance). We anticipate a 3 dB increase in received power from a ground reflection. We found the maximum detectable distance to be 18.3 meters (60 feet). This exceeds our estimated maximum detection distance by 2.5 dB.

Next, we placed the antenna over a large ground plane (approximately 2 feet square) and observed the maximum detection increase to 20.5 meters (67 feet). The difference of about 1 dB change in directivity agrees with predictions based on simulation. Given those results, we would predict a freespace maximum detection distance of 12.9 and 14.5 meters (42 and 47 feet) without and with a large ground plane, respectively.

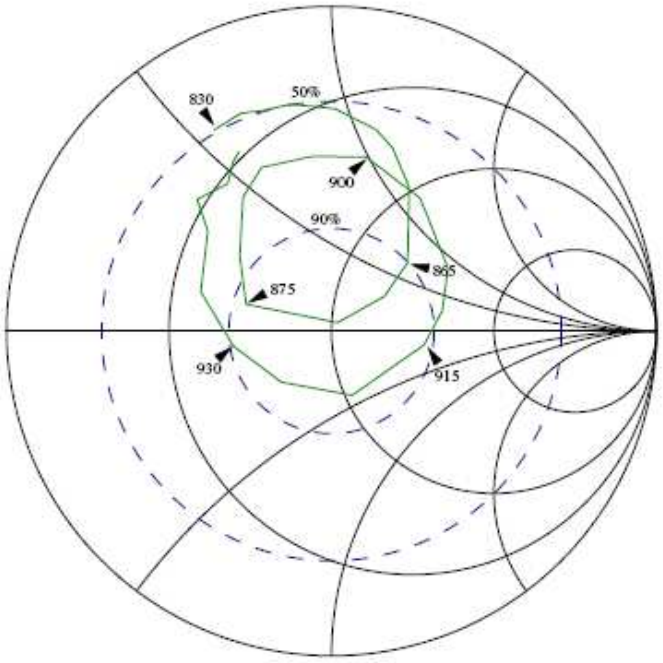

Fig.20: Power Wave Smith chart of measure antenna impedance normalized to 13-j65. The 90% and 50% power transfer efficiency circles are also plotted.

As a second method of validation, we placed the tag two meters from a different reader (Samsys) in a laboratory environment. The tag was placed on an expanded polystyrene block 2 meters from the reader. The reader frequency was fixed to 915 MHz, and the power was varied until we found the minimum power that was able to read the tag. Based on - 13 dBm IC turn-on power, we would predict the minimum reader power would be 16.5 dBm. We measured 17.0 dBm. Given that result, we would predict a free-space read distance of 9.3 meters (32 feet). However, we have reason to believe that the system is not forward-link limited [5], and thus results in a conservative estimate.

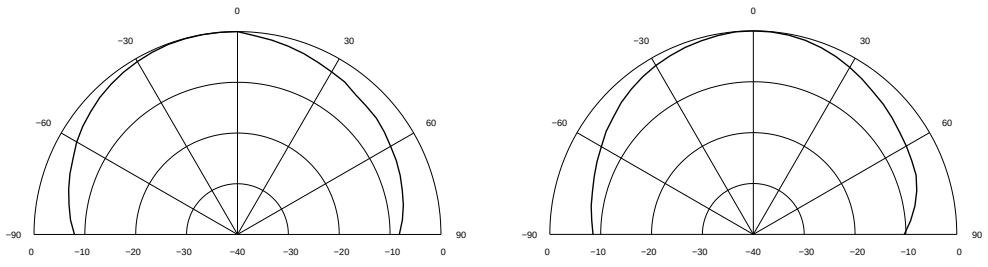

(a) E-plane, 870 Mhz (b) H-plane, 870 Mhz

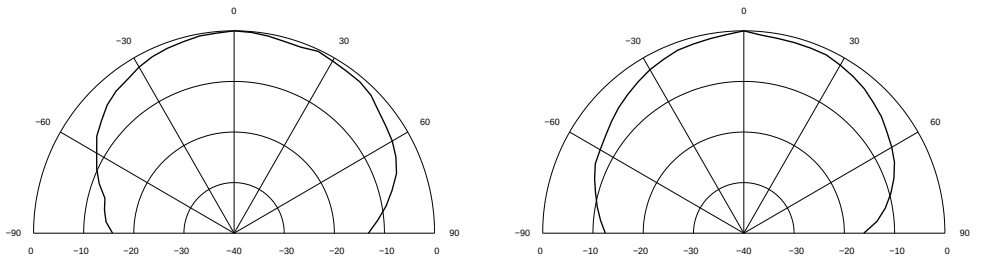

(a) E-plane, 915 Mhz (b) H-plane, 915 Mhz

Fig. 21 Radiation pattern

We can conclude that the free-space read distance will be between 9.3 and 13.1 meters, and 10.4 and 14.7 meters on a large metal ground plane. Matched

linearly polarized reader antennas will add 3 dB of link margin. The measured radiation pattern of the tag in both the E- and H-plane at both 870 and 915 MHz are shown in Fig. 21. Since the antenna is dual-polarized, the planes reverse at the two resonant frequencies. The radiation pattern was measured with the same ground plane mentioned before (not infinite), and show good agreement with simulated results.

4. Antenna and Matching Network Analysis

In section 3, we proposed a design for a dual-resonant RFID tag. We presented impedance measurements, radiation patterns for the E-plane and H-plane, and read-distance measurements. The antenna was simulated using a finite element method code. This method does not provide insight to the working of the matching network. Also, the antenna geometry was not simple enough to apply a rigorous theoretical analysis. In this section, we modify the earlier design , namely by implementing a CPW-like structure for the feed and the matching circuit. The goal is to enable us to subject the antenna and matching circuit to a rigorous analysis and also synthesize a simple circuit model for the same, which predicts the impedance and performance curves of the tag. In Section 4.1, we introduce the modified design. In Section 4.2, we present the circuit model along with impedance and performance measurements. In Section 4.3, we present a polarization model derived from the circuit model along with data and results.

4.1 Modified Design

The inspiration for the antenna comes from the three factors mentioned in Section 3. First, from the dual-resonant rectangular antennas closely exciting the TM_{01} and TM_{10} modes and feeding in such a way to excite both modes [20]. Second, we draw from the use of microstrip transmission lines to build a completely planar microstrip antenna [12]. Third, we note the use of a cross-shaped slot in a microstrip

antenna originally used to reduce the size of the antenna [21], but instead we use the cross as space to place the matching circuit and IC. We use the slots to place a microstrip CPW transmission line for feeding and impedance matching. Fig. 22 shows the modified design. The darkened area represents the metalized area. As before, the antenna was designed to operate over a polypropylene substrate with h = 5.08 mm and a dielectric constant of 2.26 and loss tangent estimated to be 0.001. The substrate and ground plane are 6 inches (15.2 cm) square. We used the same IC whose series impedance was found to be 13-j65.

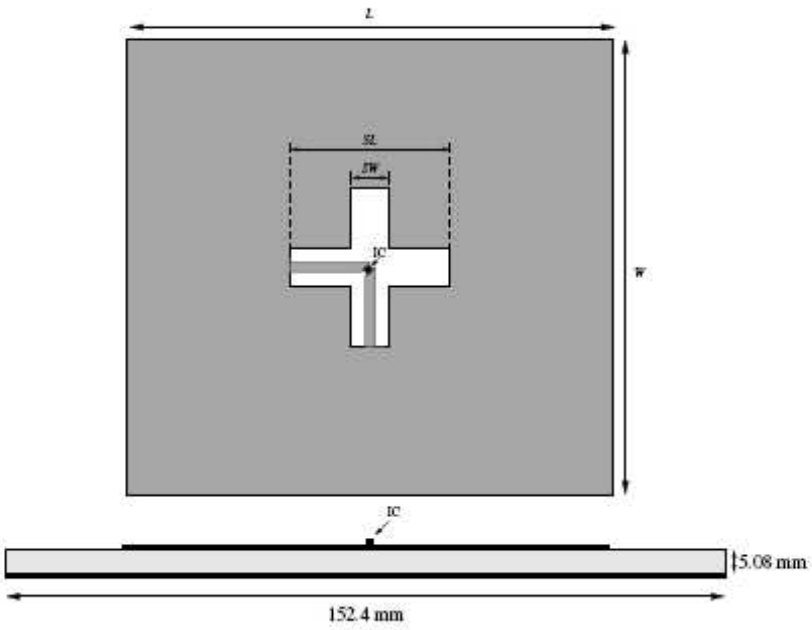

Fig. 22: Antenna schematic. L = 108 mm, W = 102 mm, SL = 20 mm, SW = 9 mm.

To develop the antenna, we can start with dimensions of a rectangular microstrip antenna that will excite the TM_{01} and TM_{10} modes at the desired frequency using, e.g., a cavity model [35]. Here, we demonstrate with resonances at 867 and 915

MHz. We can determine the cross slot lengths by modeling the feed as an inset feed which we will discuss in detail in Section 4.2. We found the cross slot lengths to be 20 mm to yield a resonant resistance of 16 Ohms (slightly larger than 13 Ohms for improved bandwidth). Once the cross dimension is chosen, the antenna length and width are modified manually to resonate at the desired frequencies. The slot length prescribes two transmission line lengths totaling 17.8 mm.

4.2. Circuit Model

To predict the antenna impedance, we constructed a simple circuit model with the component values synthesized from the physical parameters. We model each antenna resonance as a parallel LRC circuit and feed them in series transformed by a short transmission line which can be modeled as an inductor. Since the length is relatively short and the characteristic impedance large compared to the load, we use the approximation that $Z_{in} = Z_l + jZ_0\beta l$, where Z_l is the feed impedance, l = 17.8 mm, and β= 24.15. In section, 2.7.2, we presented equations to find the characteristic impedance of a conductor-backed CPW. To achieve the desired reactance, we chose Z_0 = 155 Ohms, which can be achieved with a transmission line width of 1 mm and SW = 9 mm . ICs with lower Q can be matched this way by reducing Z_0; higher Q ICs may require additional meandering of the transmission line to increase the reactance. In the subsequent subsections, the method for calculating the Q and radiating input resistance will be explained. We will conclude with the complete circuit model and measured results for impedance and performance.

4.2.1 Quality factor and Resonant Frequency

We know that we want a resistance of about 16 ohms and resonances at 867 and 915 MHz. If we know the resistance, resonant frequency and the quality factor, we can determine the values of L and C for the parallel circuit. We have, for a parallel LRC circuit, $f_0 = \frac{1}{2\pi\sqrt{LC}}$ and $Q = R\left(\frac{L}{C}\right)^{-1/2}$. Therefore, $L = \frac{R}{Q\omega_0}$ and $C = \frac{Q}{R\omega_0}$.

In our case, we find that $Q \approx Q_{rad}$ since losses due to conduction and dielectric are very low. We can modify the equations presented in section 2.5.5 for q-factor due to radiation loss to be

$$Q = \frac{\omega\varepsilon_0\varepsilon_r LW}{2hG_{rad}}$$

where

$$G_{rad} = 2[G_1 + G_{12}]$$

$$G_1 = \frac{1}{90}\left(\frac{W}{\lambda_0}\right)^2$$

$$G_{12} = \frac{1}{120\pi^2}\int_0^{\pi}\left[\frac{\sin\left(\frac{k0W}{2}\cos\theta\right)}{\cos\theta}\right]^2 J_0(k_0 L\sin\theta)\sin^3\theta d\theta .$$

We estimate G_{rad} is 2.6 mS at 867 MHz and 3.3 mS at 915 MHz, yielding Q_1=45 and Q_2=38 at 867 MHz and 915 MHz respectively.

4.2.2 Input Resistance

In order to estimate the resistance, we can treat the CPW feed as an inset feed as shown in Fig. 23. We know that the edge resistance is $R_{in(y=y0)}=R_{rad}=1/G_{rad}$. Using the expression presented in Section 2.5.4, the input resistance at a distance y_0 is given by the equation.

$$R_{in(y=y_0)} = R_{in(y=0)} \cos^2\left(\frac{\pi y_0}{L_1}\right)$$

where L_1 is the physical length of the antenna shown in Fig. 23 and y_0 is the distance from the edge.

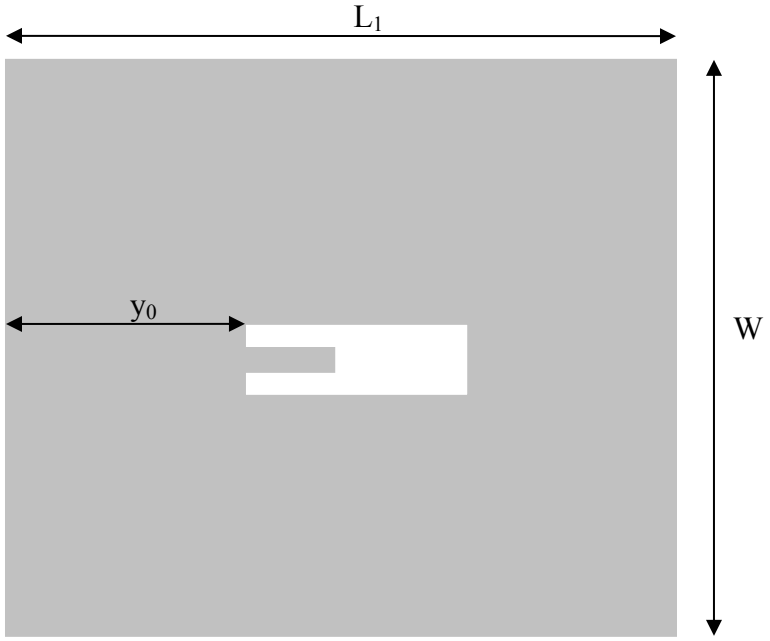

Fig. 23: Rectangular patch with CPW inset feed

Since our antenna design employs a cross slot, it increases the electrical length of the antenna. This means that if Antenna 1 in Fig. 23 and Antenna 2 in Fig. 24 are

designed such that they have the same resonant frequency, the physical length L_1 of Antenna 1 will be greater than the physical length, L_2 of Antenna 2, but their electrical lengths will be the same. We can now define an effective length, for our antenna design in Fig. 24, which is equivalent to a physical length of the antenna configuration shown in Fig. 23, i.e., $L_{eff}=L_1$. This approximation holds since the radiation resistance is mostly dependent on the width of the patch. [Mutual conductance is dependent on the length of the patch but since it is small, it can be neglected.]. We find the value of L_{eff} to be 111 mm and 108 mm for 867 and 915 MHz respectively. Therefore, we can modify the equation for the input resistance to be

$$R_{in(y=y_0)} = R_{in(y=0)} \cos^2\left(\frac{\pi y_0}{L_{eff}}\right)$$

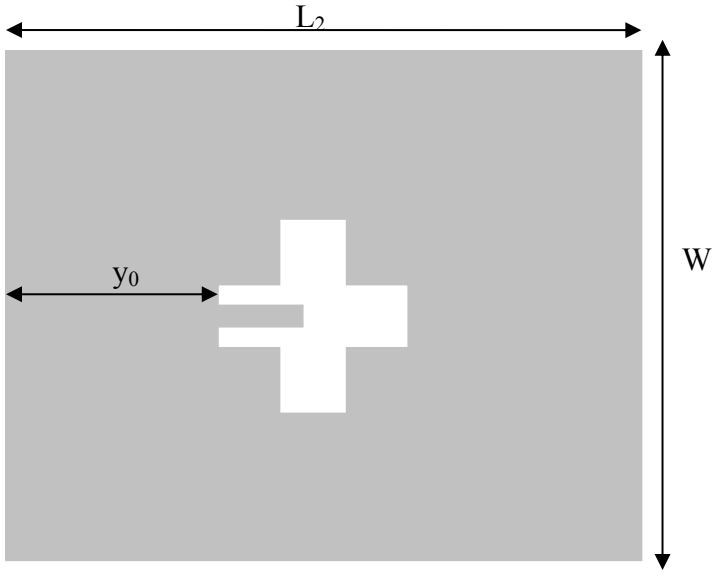

Fig. 24: Cargo tag with inset feed.

We find that the value of the predicted resistance using this equation is approximately 39 Ohms. However, a finite element method tool analysis and measured results show us that the resistance when transformed along the length of the feed is significantly lower with a value of 16 Ohms. Therefore, by modeling the feed as a conductor backed CPW, we can predict the correct reactance but not the resistance. It has been sited [36] that the gap width between the rectangular patch and the feed affects the feed resistance. In Chapter 5, we will discuss in detail the feed structure. For the purpose of presenting an accurate circuit model, we use the value of the resistance to be 16 Ohms at 867 and 15 ohms at 915 MHz respectively as simulated by our finite element tool.

We find that L_1= 68 pH and C_1= 445 pF at 867 MHz and L_2= 65 pH and C_2= 521 pF at 915 MHz. The grounded CPW is modeled as two 6 nH inductors. The resulting circuit is given in Fig. 25. The total impedance for a range of frequencies can be computed by taking the two parallel resonant circuits in series with the two inductors used to model the feed. The predicted impedance from 840 to 940 MHz is plotted in Fig. 26.

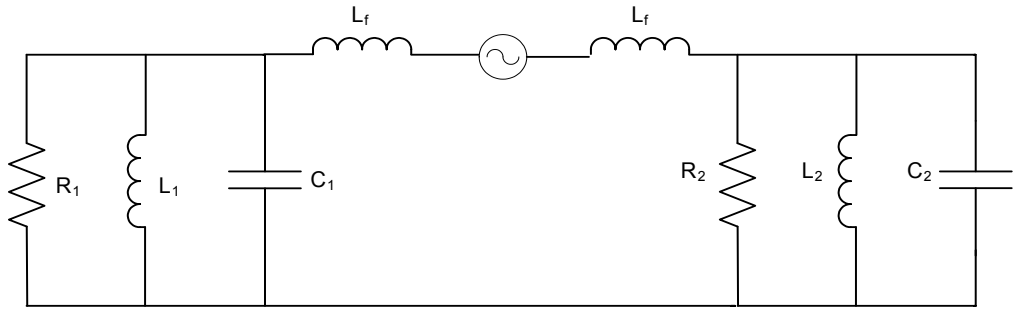

Fig. 25: Circuit model of antenna. R_1 =16 Ohms, R_2 = 15 Ohms, L_f = 6.0 nH, L_1 = 68 pH, C_1 = 445 pF, L_2 = 65 pH, C_2 = 521 pF.

4.2.3 Impedance and Performance Measurements

In this section we present the measured results of impedance and performance for the tag specifications given above. The same chip balun used for the initial design was used to measure the impedance using a network analyzer. We present the impedance predicted from our circuit model and measured impedance in Fig. 26. The results show excellent agreement given the number of approximations made in this model and the inaccuracies of the balun measurements.

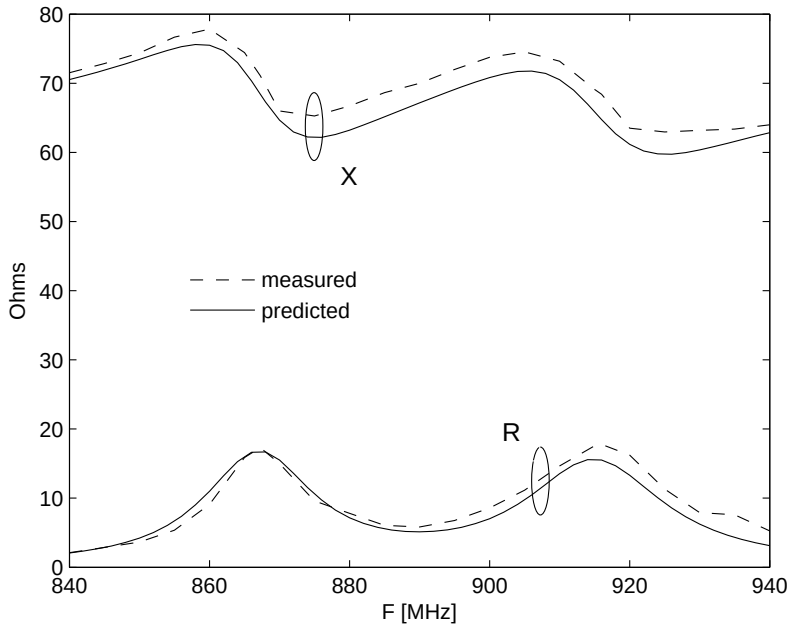

Fig. 26: Measured impedance of antenna and predicted impedance using the circuit model.

Next, we placed an IC on the antenna, placed the antenna in front of a commodity reader at a distance of 2 meters and measured the minimum amount of power required to stimulate the tag at various frequencies from 900 to 945 MHz.

Using the power transfer efficiency expression $\tau = \frac{4R_a R_c}{|Z_a + Z_c|^2}$ where Z_a and Z_c are the antenna and chip impedances respectively, we can calculate the power transfer efficiency over the range of frequencies from 900 to 945 MHz. Z_a is determined from the circuit model and Z_c is 13-*j*65. Since the power transfer efficiency tells us how efficiently power is transferred from the chip to the tag, it can be compared with the turn-on power of the tag at different frequencies. We compared the tag turn-on power vs. frequency measured by the reader and that predicted by the circuit model. The results are shown in Fig. 27 normalized so that the maximum performance for each case is 0 dB.

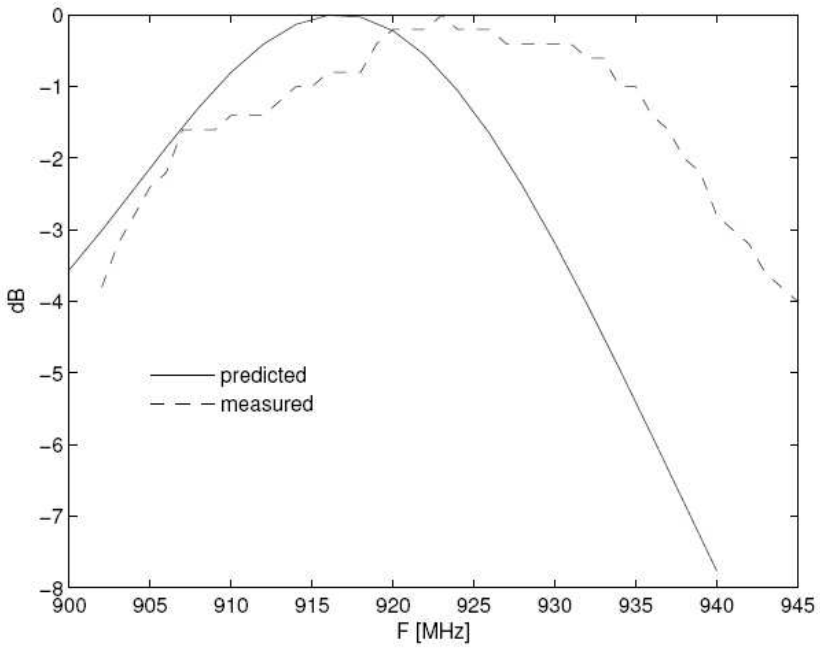

Fig. 27: Predicted and measured performance vs. frequency.

The results show a distinct shift in peak performance from resonance: peak performance occurs at the minimum reactance. Either the antenna reactance is too large or the estimated IC impedance is too small. An additional design iteration should decrease Z_0 moderately until an alignment of resonance and peak performance is achieved.

4.3 Polarization

Though the antenna is essentially linearly polarized at 867 and 915 MHz, off-resonance, the antenna tends to become slightly elliptically polarized. Also, from the circuit model, we can see that the currents will have a phase difference. In this section, we will use our circuit model to analyze this effect for broadside polarization by defining a ratio of powers for vertical and horizontal polarization which can be determined by applying circuit theory to our equivalent circuit model of the antenna under consideration. We will compare our predictions with measurements.

4.3.1 Analysis

To characterize the polarization of the antenna, we first need to find the electric fields transmitted by the antenna. The transmission line model uses the aperture field approach to find the radiation fields of a rectangular microstrip antenna. In the transmission line model, two slots at the radiating edge are considered. The two parallel slots have a width h and length W and are separated by a distance L. The antenna is linearly polarized with the direction of the electric field along the length of

the patch. The voltage across the radiating slot is V_0. When the antenna is placed broadside, i.e., when θ=0 and φ=0, the electric field is given by [32]

$$E = -jk_0 V_0 W \frac{e^{-jk_0 r}}{2\pi r} F_3$$

where,

$$F_3 = \frac{2\sqrt{\varepsilon_r}}{\sqrt{\varepsilon_r} - j\varepsilon_r \cot(k_0 h\sqrt{\varepsilon_r})}.$$

Since our antenna is dual resonant by exciting two modes, we have two sets of radiating slots, one which is linearly polarized vertically and one which is linearly polarized horizontally. The voltage across the vertically linearly polarized slots is V_V and that across the horizontally linearly polarized slots is V_H. This is illustrated in Fig. 28. The fields for horizontal and vertical polarized slots can be written as

$$E_H = -jk_0 V_H W_H \frac{e^{-jk_0 r}}{2\pi r} F_3$$

$$E_V = -jk_0 V_V W_V \frac{e^{-jk_0 r}}{2\pi r} F_3$$

For our antenna, $W_V \approx W_H$. Other than the voltage developed across the slots, all other parameters are the same for both set of radiating slots. If we take the ratio of the two fields we get,

$$\frac{E_V}{E_H} = \frac{V_V}{V_H}$$

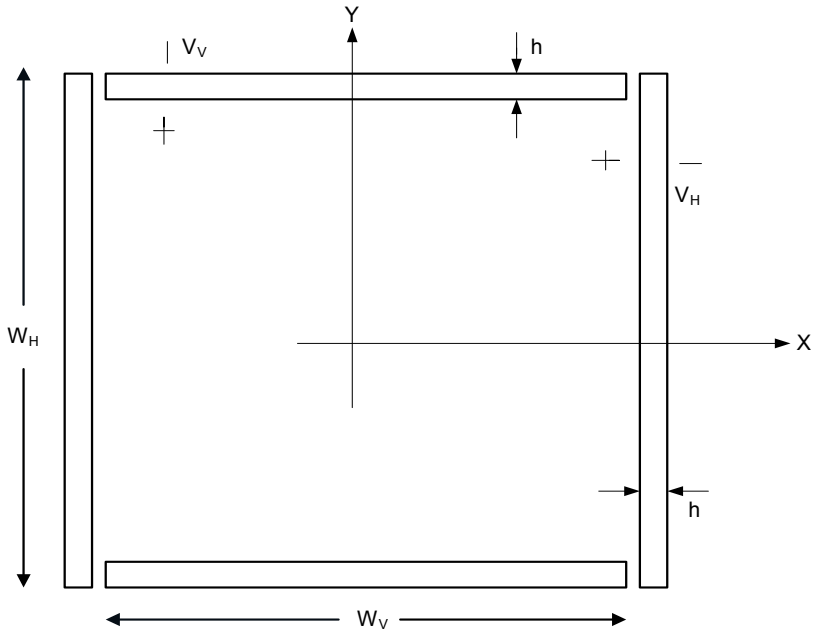

Fig. 28: Aperture model for the cargo tag.

Using our circuit model and applying circuit theory, we can find the voltage induced across the chip resistance for vertical and horizontal polarization. The models are shown in Fig. 29 and Fig. 30. R_c=350 Ohms and C_c=2.5 pF. All other resistance, capacitance and inductances are same as those given in Fig. 25.

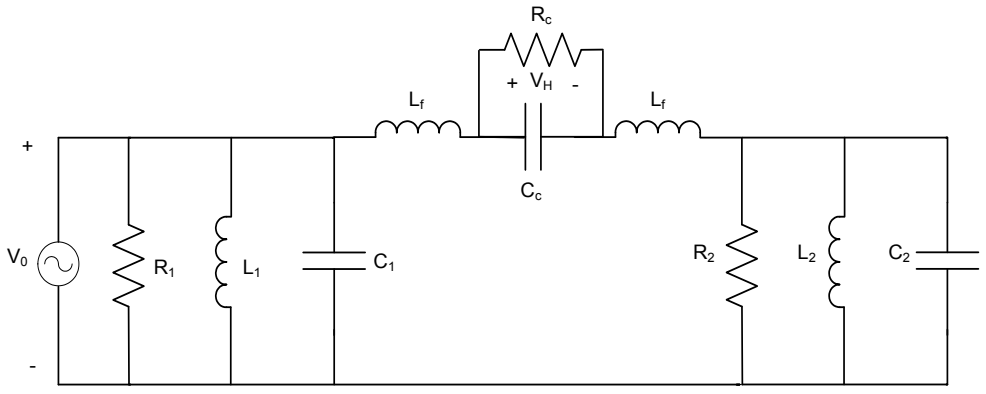

Fig. 29: Polarization model for horizontal polarization

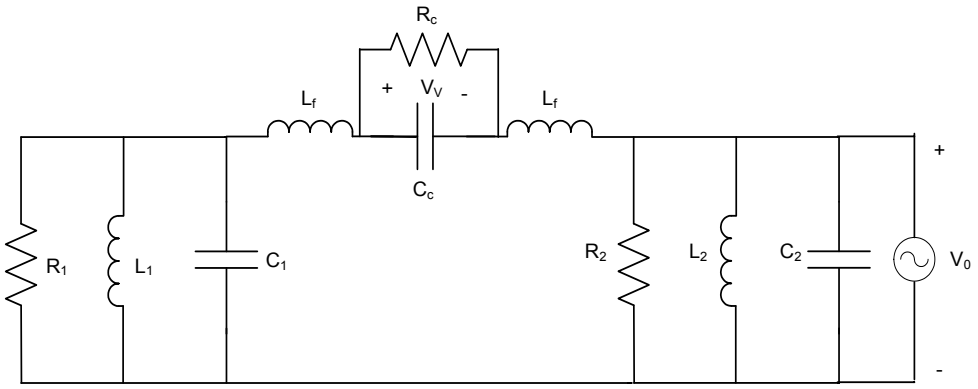

Fig. 30: Polarization model for vertical polarization

We assume a 1 V voltage source for V_0 in both cases. We know that the voltage across parallel circuits is the same and for impedances in series, we can use the voltage divider rule to determine the voltage developed across each impedance. Once we find V_V and V_H, we can find the ratio of the powers as

$$\zeta = \frac{P_V}{P_H} = \frac{V_V^{\,2}}{V_H^{\,2}}.$$

We call this ratio as the vertical to horizontal polarization power ratio. It can be expressed in dB as $10\log P_V/P_H$. The predicted power ratio plot in dB is shown in Fig. 31 along with the measured results.

4.3.2 Measurements and Results

We placed the antenna with the IC in front of a commodity reader at a distance of 2 meters and measured the minimum amount of power required to stimulate the tag at various frequencies from 900 to 945 MHz at an angle of 0 degrees. Next, we rotated the angle by 90 degrees and performed the same

experiment. This gives us the turn on power for vertical and horizontal polarizations. The graph shows the predicted and the measured vertical to horizontal polarization power ratio. We can observe from the graph that though measured and predicted results do not line up exactly, they follow a similar trend. Thus, we conclude that our circuit model gives us a good approximation of ξ.

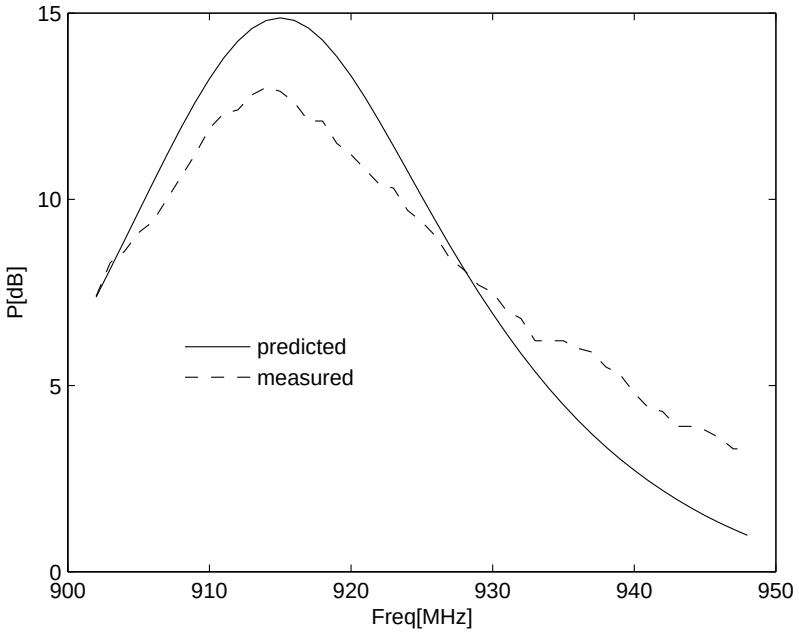

Fig. 31: Measured vs. predicted vertical to horizontal polarization power ratio

5. Ongoing Work: Feed Structure Analysis

As we mentioned in Section 4.2.2, the resistance decreased from 39 ohms to 16 ohms from the inset feed point to the input of the CPW feed structure. Further analysis showed that the resistance continues to decrease with the increase in the feed length and increases with reduction in the feed length. Fig. 32 shows the geometry of a rectangular patch with a single slot. Fig. 33 shows the geometry of a rectangular patch with a cross slot. In both cases, we fed the antenna in such a way as to excite the TM_{01} mode to get a resonance at about 867 MHz. The variation of the resistance with the change in the feed length for the rectangular patch with cross slot and single slot is shown in Fig. 34. We see similar results when exciting the TM_{10} mode. This leads us to believe that the CPW feed structure does not behave as a coplanar waveguide transmission line driven in the odd mode. We hypothesize that the decrease in resistance is due to coupling between the feed and the rectangular patch. In this section, we discuss various simulations and the results to validate our hypothesis. However, we will find that our hypothesis is invalidated by the results. We make another hypothesis and discuss further experiments that could be carried out to verify the hypothesis.

To keep our analysis simple, we will use the rectangular patch microstrip antenna with a single slot with the dimensions given in Fig. 32. Using HFSS, a finite element method tool, we will first model the region shown by the solid lines in Fig. 32. The same dielectric substrate with thickness 5.08 mm was used. This is similar to modeling the coupling between three microstrip transmission lines.

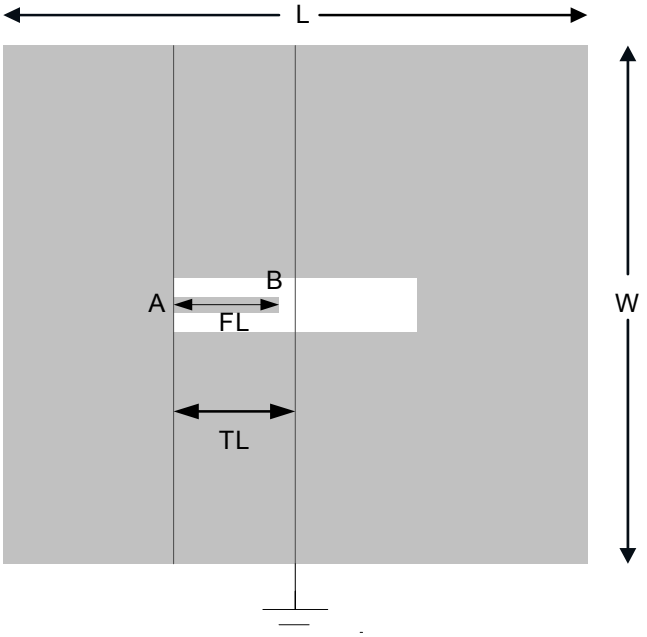

Fig. 32: Rectangular patch antenna with a single slot. Exciting the TM_{01} mode to get resonance at 867 MHz. L=108 mm, W=102 mm, TL=10 mm, FL=8.5 mm.

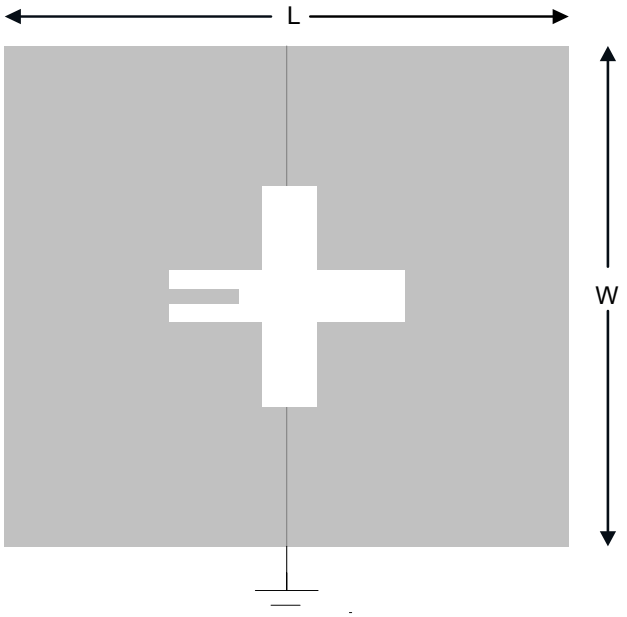

Fig. 33: Rectangular patch antenna with a cross slot. Exciting the TM_{01} mode to get resonance at 867 MHz. L=108 mm, W=102 mm.

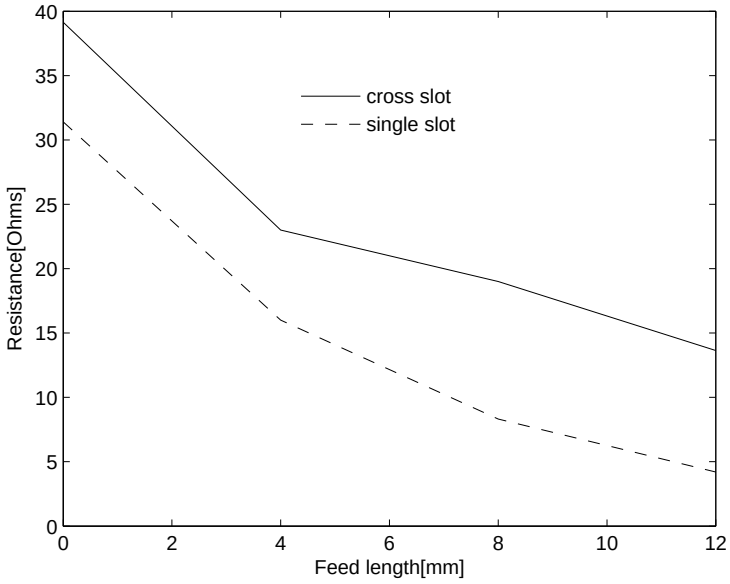

Fig. 34: Variation of the input resistance with change in length for rectangular patch with single slot and cross slot with the TM_{01} mode being excited.

Fig. 35 shows the HFSS model of the three lines. Lines 1 and 3 are identical and Line 2 is the feed. Lines 1 and 2 are 10 mm long and Line 2 is 8.5 mm long. At ports 1, 2 and 3, we placed 40 ohm loads and grounded ports 4 and 6. A lumped port was placed at port 5 to measure the input impedance. We found the input impedance at port 5 to be $45+j56$. The resistance did not change significantly over the length of transmission line. In fact, the resistance increased by 5 Ohms. We see only a significant change in the reactance from point A to B [0 to 56 Ohms].

Next, we used a single lumped port to drive the three lines, grounded ports 4 and 6 and placed a lumped port at port 5. We retrieved the two-port network's Z-parameters from the simulation and calculated the input impedance with a 40 ohm

load. The calculated input impedance was found to be 43+*j*45. We still observed that the resistance did not decrease from A to B.

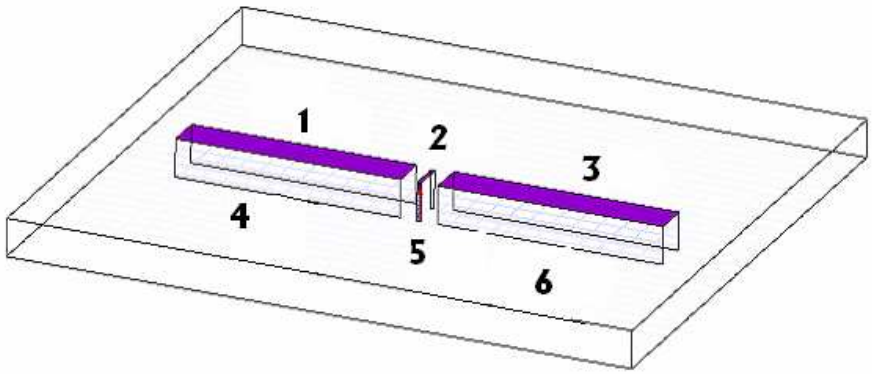

Fig. 35: HFSS simulation model

Finally, to check that the resistance was indeed the same everywhere just before and after the feed point, we probed the impedance at the six different locations over a small strip ε shown in Fig. 36. We observed a slight change in the resistance from point *a* to *b* and *b* to *c* and from *d* to *e* and *e* to *f* (about 10 Ohms). We used these new values in the simulations. Instead of placing 40 Ohm loads at ports 1, 2, and 3, we placed 30 Ohm loads at ports 1 and 3 and a 40 Ohm load at port 2. The input impedance at port 5 was found to be 45+*j*55. The difference in the resistance from *a* to *b* and *b* to *c* did not change the input impedance significantly. All these results lead us to believe that coupling is not causing the reduction in the resistance as the feed length increases. It must be due to the discontinuities which arise in the

region ε and higher order modes which have not been explored in the scope of this thesis.

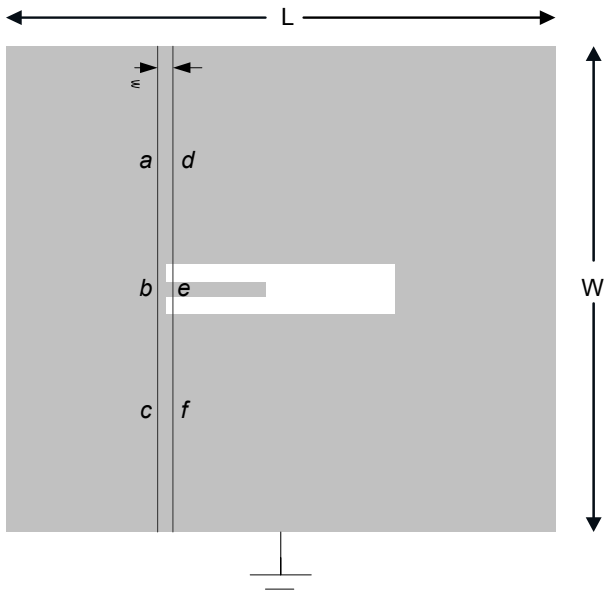

Fig. 36: Resistance values were checked at points *a, b, c, d, e* and *f*.

A possible method for confirming that the decrease in the input resistance is due to discontinuities and higher order modes is to set up a HFSS simulation with the geometry shown in Fig. 37. In this way, we can model the region just before the discontinuities occur and find out how it affects the input resistance. At 1 and 2 a lumped port can be placed to determine the z parameters of the 2-port network while grounding 3 and 4. With a 40 ohm load, the input impedance at 2 can be determined. We might be able to account for the decrease in resistance.

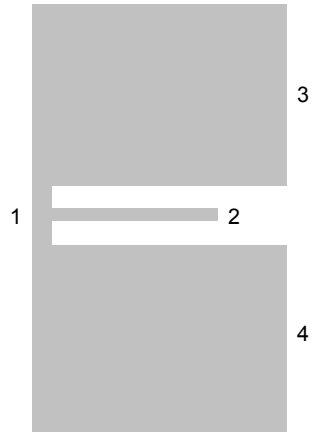

Fig. 37: Geometry for HFSS Simulation to model discontinuities in the rectangular patch.

We have analyzed the feed structure to the best of our ability in the stipulated time. From our analysis, we can make the following observations, deductions and conclusions:

- We can accurately predict the resistance at the inset feed point.
- Along the length of the feed, the resistance decreases.
- The decrease in resistance cannot be accounted for by modeling the feed as a coplanar waveguide driven in the odd mode.
- The decrease in resistance is not due to coupling of the feed with the neighboring transmission lines.
- There are discontinuities present just before the feed which we have not accounted for in our simulation models with the three microstrip lines.
- There are higher order modes that may be present which we have neglected in our models.
- These discontinuities and higher order modes might be the cause for the decrease in resistance which can be explored further.

6. Conclusion and Future Work

In this thesis, we presented a novel, high-performing dual-resonant, dual-polarized UHF RFID tag for tagging large cargo containers. The antenna is designed to perform efficiently between 860-870 MHz and 902-928 MHz frequency bands, but it can be easily modified to operate at any two of the three frequency bands used worldwide. The antenna is a completely planar structure so that it may be easily manufactured using inlays.

We also showed measured impedance results using the power wave Smith chart, showing excellent power transfer efficiency over the frequency bands of interest. We also measured the performance of the tag using a TI chip and commodity reader over 900 and 945 MHz.

We analyzed the antenna rigorously. We were successful to a certain degree. We synthesized an equivalent circuit model for the antenna and matching circuit for predicting the antenna impedance. We showed that the polarization can also be characterized using this model. We presented measured and predicted impedance and performance results for the proposed tag antenna design and polarization prediction and measurement for vertical and horizontal polarization. The measured and predicted results had good agreement except for the input resistance. Thus, we conclude that the proposed antenna design is a novel and useful UHF RFID tag that can be easily and readily commercialized. Further, with the analysis presented in this thesis, the antenna design is easy to understand and prototype.

Although we have presented a rigorous analysis of the working of the antenna and feed structure, there are still open problems regarding the feed structure. We are still not certain why the resistance decreases along the length of the feed. We believe that the work that we have done gives us some insight that higher order modes and discontinuities are the cause of the decrease in resistance. Future work may explore this concept further. Also, the accuracy of our measurements can be improved with better measurement methods.

7. References

1. S. Aroor and D.D. Deavours , " A dual-resonant microstrip-based UHF RFID' cargo' tag ," in *Proc. IEEE International Microwave Symposium*, Atlanta, GA, June 2008
2. D. M. Dobkins, The RF in RFID: Passive UHF RFID in Practice. Burlington, MA: Newnes, 2007.
3. D. M. Dobkins and S. Weigand, "Environmental effects on RFID tag antennas," in IEEE MTT-S International Microwave Symposium, Long Beach, CA, Jun. 2005, pp. 4–7.
4. J. Griffin, G. Durgin, A. Haldi, and B. Kippelin, "Radio link budgets for 915 MHz RFID antennas placed on various objects," in Proc. 2005 Texas Wireless Symposium, Austin, TX, Oct. 2005, pp. 22–26.
5. S. R. Aroor and D. D. Deavours, "Evaluation of the state of passive UHF RFID: An experimental approach," IEEE Systems Journal
6. C.A. Balanis, Antenna Theory: Analysis and Design, John Wiley & Sons, Inc, 1997.
7. W.L. Stutzman, and G.A. Thiele, Antenna Theory and Design, John Wiley & Sons, Inc, 1998.
8. Y. T. Lo, and S. W. Lee, Antenna handbook: Antenna theory, Vol.2, International Thompson Publishing, Inc, 1993.

9. Catherine, M.: 'Symbol Announces Gen 2 Tags, Converter Program.' RFID Journal, News article, May 2006.

10. Alien Technology – RFID tags, http://www.alientechnology.com/products/rfid_tags.php

11. Avery Dennison RFID: Products: Portfolio, http://www.rfid.averydennison.com/us/products_portfolio.php

12. M. Eunni, M. Sivakumar, and D. D. Deavours, "A novel planar microstrip antenna design for UHF RFID," Journal of Systemics, Cybernetics and Informatics, vol. 5, no. 1, pp. 6–10, Jan. 2007.

13. K. R. Carver and J.W. Mink ," Microstrip Antenna Technology," IEEE Transactions Antennas and Propogation, Vol. AP-29, No.1, pp 2-24, January 1981

14. J.R. James and P.S. Hall, Handbook of Microstrip Antennas, Vols. 1 and 2 , Peter Peregrinus, London, UK , 1989

15. E.H. Van Lil and A.R. Van de Capelle , " Transmission-Line model for Mutual Coupling Between Microstrip Antennas," IEEE Transactions on Antennas and Propogation, Vol. AP-32, No. 8, pp. 816-821, August 1984

16. A. G. Derneryd, " A theoretical investigation of the rectangular microstrip antenna element," IEEE Transactions Antennas and Propagation, Vol. AP-26, No.4, pp. 532-535

17. W. F. Richards , " Microstrip Antennas", Chapter 10 in Antenna Handbook: Theory, Applications and Design(Y.T. Lo and S.W. Lee, eds.), Van Nostrand reinhold Co. , New York, 1988

18. R.F. Harrington, Time- Harmonic Electromagnetic Fields, McGraw Hill Book Co., New York, pg.183, 1981

19. R. Garg, I. Bahl, P. Bhartia, and K. C. Gupta, Microstrip Lines and Slot lines, 2nd ed. Norwood, MA: Artech House, 1996.

20. J. S. Chen and K.-L. Wong, "A single-layer dual-frequency rectangular microstrip patch antenna using a single probe feed," Microwave and Optical Technology Letters, vol. 11, pp. 83–84, Feb.1996.

21. K.-L. Wong and K.-P. Yang, "Small dual-frequency microstrip antenna with cross slot," Electronics Letters, vol. 33, no. 2, pp. 83–84, Nov. 1997.

22. Wen, C.P. ," Coplanar Waveguide: A Surface Strip Transmission Line Suitable for Non-Reciprocal Gyro magnetic Device Application," IEEE Transactions, Vol. MTT-17, 1969, pp. 1087-1090.

23. H.W. Son and G.Y. Choi, " Orthogonally proximity-coupled patch antenna for passive RFID tag on metallic surfaces," *Microw. Opt. Technol. Lett*., vol.49, no.3, pp. 715-717, 2007

24. D. M. Dobkins and S.M. Weigand, " Environmental effects on RFID tag antennas," in. *IEEE Microw. Symp Dig.*, 2005, pp. 135-138

25. Klaus Finkenzeller, RFID Handbook, 2nd Edition, John Wiley and Sons Ltd, England, pp. 7-10

26. K. Kurokawa, "Power waves and the scattering matrix," IEEE Transactions on Microwave Theory and Technique, vol. 13, no. 3, pp. 194–202, Mar. 1965.

27. P. V. Nikitin, K. V. S. Rao, S. F. Lam, V. Pillai, R. Martinez, and H. Heinrich, "Power reflection coefficient analysis for complex impedances in rfid tag design," IEEE Transactions on Microwave Theory and Technique, vol. 53, no. 9, pp. 2721–2725, Sep. 2005.
28. http://www.aptsec.org/
29. P. V. Nikitin and K. V. S. Rao, "Reply to 'Comments on "Antenna design for UHF RFID tags: A review and a practical application"'," IEEE Transactions on Antennas and Propagation, vol. 54, no. 6, pp. 1906–1908, Jun. 2006.
30. Ansoft Corporation, HFSS Online Help, Ansoft Corporation, Pittsburg, PA, 2006.
31. T. Instruments, TI UHF Gen2 IC — Reference Guide, 1st ed., Dallas, TX, Jun. 2006.
32. P. Bhartia, I. Bahl, R. Garg, and A. Ittipiboon, Microstrip Antenna Design Handbook. Artech House Publishers, Nov. 2000.
33. H. Kwon and B. Lee, "Compact slotted planar inverted-F RFID tag mountable on metallic objects," Electronics Letters, vol. 41, no. 24, pp. 1308–1310, Nov. 2005.
34. http://www.jefflindsay.com/rfid3.shtml#intro- cascading of RFID tags
35. Y. Lo, D. Solomon, and W. Richards, "Theory and experiment on microstrip Antennas," IEEE Transactions on Antennas and Propagation, vol. 27, no. 2, pp. 137–145, Mar. 1979.
36. Lorena I. Basilio, Michael A. Khayat, Jeffery T. Williams, and Stuart A. Long, " The Dependence of the Input Impedance on Feed Position Probe and Microstrip

Line-Fed Patch Antennas", IEEE Transactions on Antennas and Propagation, Vol. 49, no. 1, Jan. 2001

37. http://www.worldshipping.org/

38. http://s3.amazonaws.com/energy-futures.com/port_study

39. http://www.rfidjournal.com/article/view/26/1/1

40. Mark Roberti, "Consensus Reached on EPC Gen2 ", RFID Journal, June 24, 2004

41. http://www.rfidjournal.com/magazine/article/2765